



## Article

# Assessing the Applicability of Three Precipitation Products, IMERG, GSMaP, and ERA5, in China over the Last Two Decades

Hongwu Zhou <sup>1,†</sup> , Shan Ning <sup>1,†</sup> , Da Li <sup>1,\*</sup>, Xishan Pan <sup>2</sup>, Qiao Li <sup>1</sup>, Min Zhao <sup>1</sup> and Xiao Tang <sup>1</sup>

<sup>1</sup> School of Marine Science and Engineering, Nanjing Normal University, Nanjing 210023, China; zhouhwu@njnu.edu.cn (H.Z.); ns03@njnu.edu.cn (S.N.); liqiao@njnu.edu.cn (Q.L.); zhaomin@njnu.edu.cn (M.Z.); tangxiao@nnu.edu.cn (X.T.)

<sup>2</sup> Tidal Flat Research Center of Jiangsu Province, Nanjing 210023, China; pxs0702@sina.com

\* Correspondence: lida@nju.edu.cn

† These authors contributed equally to this work.

**Abstract:** The accuracy of gridded precipitation products is uncertain in different temporal and spatial dimensions. Analyzing the applicability of precipitation products is a prerequisite before applying them to hydrometeorological and other related research. In this study, we selected three gridded precipitation products, Integrated Multi-satellitE Retrievals for Global Precipitation Measurement (IMERG), Global Satellite Mapping of Precipitation (GSMaP), and the fifth generation of atmospheric reanalysis of the European Centre for Medium-Range Weather Forecasts (ERA5), including their data from 2001 to 2020. Using the data from 699 ground observation stations, we evaluated the applicability of these three precipitation products in China. Based on five statistical and five classification indicators, we first assessed the applicability of the three precipitation products on daily, monthly, and annual time scales, respectively, and then evaluated their applicability in different spatial dimensions, including basins, agriculture, and geomorphology. The results showed that: (1) IMERG data had the best accuracy on annual and monthly time scales, with both correlation coefficient (CC) values greater than 0.95 and Kling–Gupta efficiency (KGE) values greater than 0.90. On a daily time scale, the accuracy of all three precipitation products differed when statistical or categorical indicators were considered alone. However, the applicability of IMERG data was best among the three precipitation products when both types of indicators were considered. (2) The accuracy of the three precipitation products gradually decreased along the southeast–northwest direction. The applicability of ERA5 data was better in northern regions than in other regions in China, especially in arid and semi-arid regions in northern China. The applicability of IMERG data was better in southern regions with more precipitation and in high-altitude regions than in other regions in China. (3) The applicability of the three precipitation products in plain areas was generally better than in mountain areas. Among them, ERA5 data were more accurate in plain areas, while IMERG data were more accurate in mountain areas. This study can provide a reference for the selection of data sources of gridded precipitation products in different time scales and spatial dimensions in China.

**Keywords:** applicability; gridded precipitation product; geomorphology; agriculture; last two decades; China



**Citation:** Zhou, H.; Ning, S.; Li, D.; Pan, X.; Li, Q.; Zhao, M.; Tang, X. Assessing the Applicability of Three Precipitation Products, IMERG, GSMaP, and ERA5, in China over the Last Two Decades. *Remote Sens.* **2023**, *15*, 4154. <https://doi.org/10.3390/rs15174154>

Academic Editors: John Kalogiros, Jianzhong Lu and Marios Anagnostou

Received: 18 July 2023

Revised: 17 August 2023

Accepted: 22 August 2023

Published: 24 August 2023



**Copyright:** © 2023 by the authors. Licensee MDPI, Basel, Switzerland. This article is an open access article distributed under the terms and conditions of the Creative Commons Attribution (CC BY) license (<https://creativecommons.org/licenses/by/4.0/>).

## 1. Introduction

Precipitation, as an important component of the global water vapor cycle and a fundamental driver of hydrological processes, plays an important role in exchanging energy and maintaining ecological balance. Uncertainty in the temporal and spatial distribution of precipitation can lead to extreme weather events such as heavy rainfall and droughts. Local heavy rainfall can easily trigger floods, affecting terrestrial hydrological cycles [1,2]. Therefore, obtaining accurate precipitation information is important in the

fields of forecasting, water resource management, agricultural production, and drought and flood disaster monitoring.

There are three methods used to obtain precipitation data. The first method is through the use of rain gauges, which is considered to be the most accurate precipitation measurement method and is often used as the ground truth value to evaluate the performance of other precipitation measurement methods [3]. However, the limited number of ground observation stations makes it difficult to capture the large-scale temporal and spatial variability of precipitation [4]. The second method involves meteorological radar, which mainly utilizes the reflection and scattering of precipitation particles to estimate the amount of the precipitation. Meteorological radar has a larger monitoring range than rain gauges, but this method may have the problem of occlusion in the case of complex terrain and high-rise buildings [5]. The third method is by remote sensing, which provides gridded precipitation data on a global scale [6]. Currently, there are many gridded precipitation products obtained using remote sensing, such as Tropical Rainfall Measuring Mission (TRMM) [7,8], Asian Precipitation-Highly Resolved Observational Data Integration Towards Evaluation of Water Resources (APHRODITE) [9,10], Integrated Multi-satellitE Retrievals for Global Precipitation Measurement (GPM) (IMERG) [11,12], Climate Prediction Center Morphing Technique (CMORPH) [5], Global Satellite Mapping of Precipitation (GSMaP) [13,14], and the fifth generation of atmospheric reanalysis of the European Centre for Medium-Range Weather Forecasts (ECMWF) (ERA5) [15,16]. These products can be divided into three categories: satellite data (infrared observations, passive microwave observations, soil moisture observations, etc.), e.g., TRMM, IMERG, GSMaP; the combination of different data sources (satellite precipitation estimates, reanalysis precipitation products, observational data, etc.), e.g., APHRODITE, CMORPH; and the creation of reanalysis products using atmospheric physical models combined with reference data [4], such as ERA5. These gridded precipitation products cover different time series, time scales, spatial dimensions, and spatial coverage. However, they are mainly affected by inversion algorithms, local weather conditions, terrain, and sampling frequency [17,18]. Therefore, the applicability of precipitation products needs to be validated based on ground observation station data.

A large number of studies on the validation of gridded precipitation products have been conducted in different regions around the world. They are either global [13,19] or in specific countries, for example, Iran [20,21], Pakistan [6,22], India [23], United Arab Emirates [24], United States [25,26], Australia [27], Bangladesh [28], Greece [29], Italy [30,31], etc. In recent years, there have been numerous studies on applicability analysis in China (Table A1). We can see that most of the applicability analysis studies have short time series [2,12,13,17,18,32–43], generally around 5 years. There are also some studies with long time series [44–48], but most of them focus on monthly and annual scales. The time series of Tang et al. [49] and Jiang et al. [50] were relatively long, up to 18 years, with minimum hourly and daily time dimensions, but they only analyzed the climate zone in the spatial dimension. Most of the studies with short time series are also further restricted to one or some of the categories of the following regional subdivisions: administrative zone [33,36,41], topography [36,40], basin [12,13,17,42], climate [32,39,43,46,50], and geomorphologic regionalization [47]. These studies generally show that the applicability of various gridded precipitation products varies more markedly across the seasons in China, with summer being generally better than winter, and applicability being directly proportional to the size of the time scale. In terms of regional dimensions, the accuracy of precipitation products varies greatly in different regions of China, with the southern region being generally better than the northern region. Satellite precipitation products generally outperform reanalysis precipitation products, but the latter significantly perform better than the former over high-latitude regions and in winter. The applicability of IMERG\_Final is overall the highest among the various gridded precipitation products; especially, the correlation coefficients with ground observation stations are significantly better than those of other precipitation products. However, we find that there are fewer studies on the

applicability of precipitation products over long time series, and regional scale division of the whole of China in spatial analysis is relatively crude.

At present, the construction of automatic stations and the advancement of digitization in China still cannot change the actual situation of China's meteorological station network being "dense east and sparse west", and the acquisition of high-resolution precipitation data is affected by this situation [39]. China has a vast territory, crisscrossing water systems, and complex topography, and agriculture is an important pillar of China's economy. We selected three gridded precipitation products, IMERG, GSMaP, and ERA5, and evaluated the applicability of the three precipitation products first in the daily, monthly, and annual temporal dimensions, and then in the spatial dimension in terms of basins, climate, geomorphology, and agriculture, using data from ground observation stations in the Chinese region based on statistical and categorical indicators (CC, RMSE, BIAS, MAE, KGE, POD, FAR, ACC, CSI, and ETS). In this study, we aimed to answer the following questions: (1) What are the quality and applicability of the three gridded precipitation products on a daily, monthly, and annual basis for the period 2001–2020 of a long time series survey? (2) How well do precipitation products perform in terms of basins, agriculture, and geomorphologic types? Which gridded precipitation products are the most appropriate?

## 2. Study Area

Located on the west coast of the Pacific Ocean and the eastern part of the Eurasian continent, China covers a vast area of approximately 9.6 million km<sup>2</sup> [12]. China is one of the countries with the most serious soil erosion in the world, characterized by a wide distribution and large area of soil erosion. The topography of China is complex, with high topography in the west and low topography in the east, presenting a clear stepped distribution. The terrain in the eastern region is relatively flat, while the terrain towards the northwest gradually becomes complex. Located on the western part of the Pacific Ocean and influenced by complex topography and special land-sea distribution, China has a diverse climate and abundant water resources. At the same time, the types of precipitation are diverse and unevenly distributed across different temporal and spatial scales. The overall precipitation in China shows a decreasing trend from southeast to northwest [51], with most regions experiencing hot and rainy summers and cold and dry winters.

Assessing the applicability of various precipitation products in China based on ground observation station precipitation data can help facilitate related work in the fields of meteorological forecasting and hydrological monitoring. In this study, we carry out the applicability analysis of different gridded precipitation products in three aspects, including basins, agriculture, and geomorphology, to better assess the accuracy of precipitation products in regional areas. The specific classification criteria are as follows:

In this study, we considered the principles of water resource classification in China by the Resource and Environment Science and Data Center and previous related studies [12]. The Chinese region was divided into nine river basins, namely: Songhua and Liaohe River Basin (S&L RB), Haihe River Basin (Hai RB), Huaihe River Basin (Hu RB), Yellow River Basin (Yellow RB), Yangtze River Basin (Yangtze RB), Pearl River Basin (Pearl RB), Southeast Basin (Southeast B), Southwest Basin (Southwest B), and Continental Basin (Continental B). Their spatial distribution is shown in Figure 1.

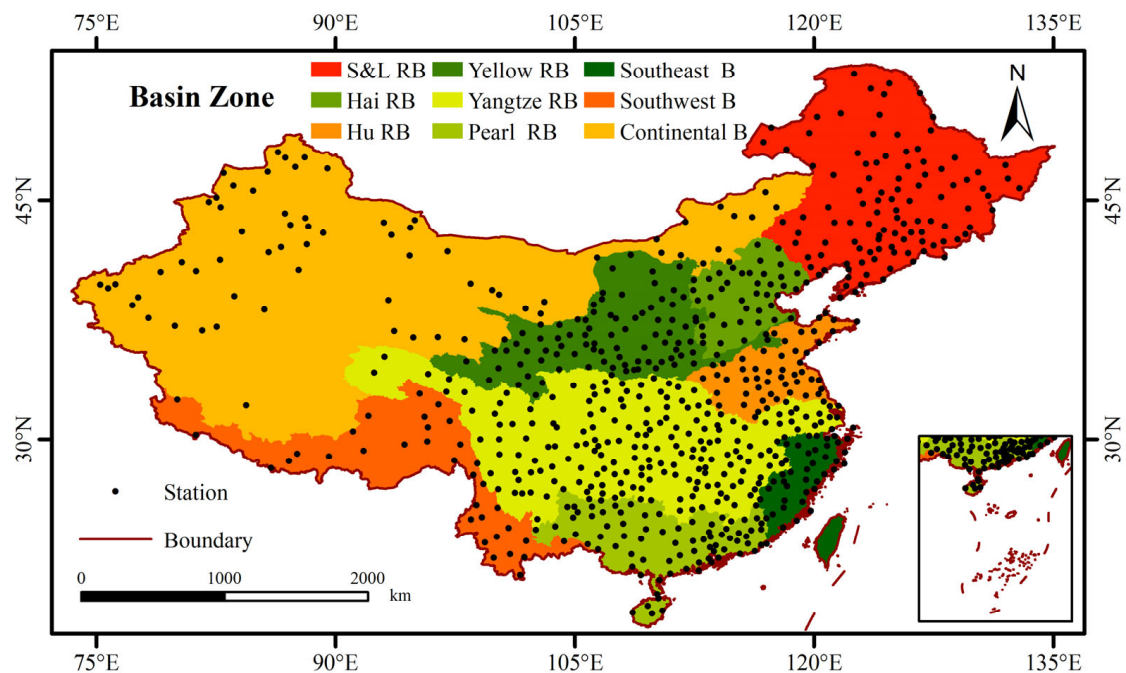


**Figure 1.** Spatial distribution of the ground observation stations in different basin zones in the studied area.

We considered the principles of the “Comprehensive Agricultural Zoning of China” and previous related studies [52], and divided the Chinese region into nine agricultural zones, namely: Northeast China Plain (NCP), Yunnan-Guizhou Plateau (YGP), northern arid and semiarid region (NASR), Southern China (SC), Sichuan Basin and surrounding region (SBSR), middle-lower Yangtze Plain (MLYP), Qinghai Tibet Plateau (QTP), Loess Plateau (LP), and Huang-Huai-Hai Plain (HHHP). Their spatial distribution is shown in Figure 2.

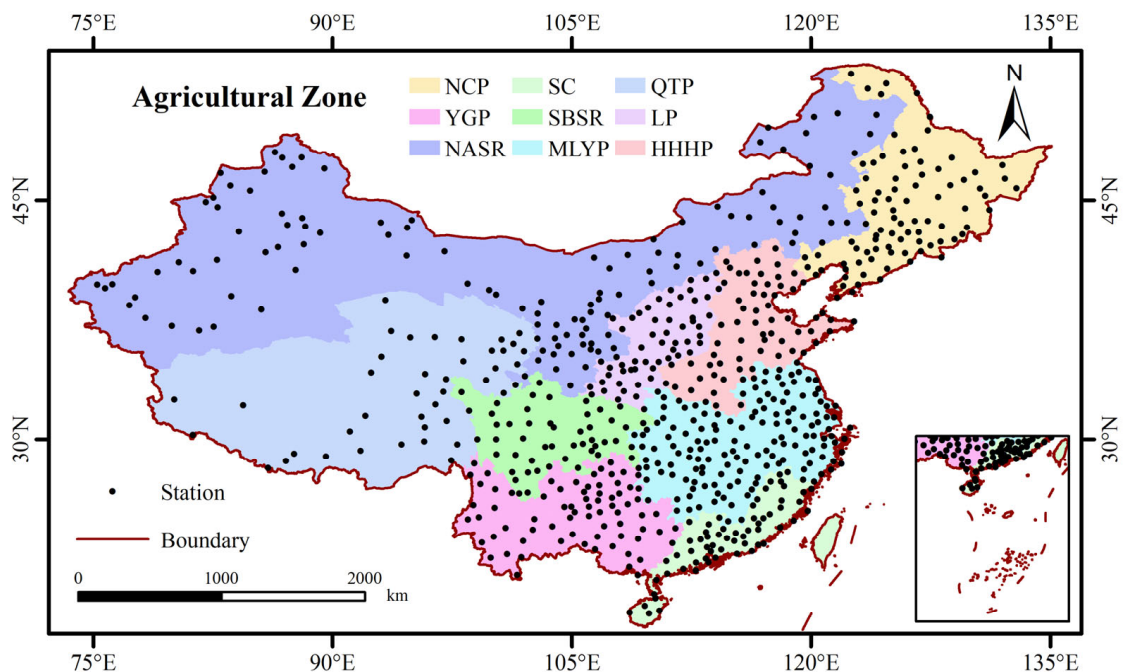


**Figure 2.** Spatial distribution of different agricultural zones in the studied area.

We referred to the principles of landform classification in China by the Resource and Environment Science and Data Center and previous related studies [8], and divided the Chinese region into seven geomorphologic types, namely: plains, platforms, hills, small undulating mountains (SUM), medium undulating mountains (MUM), large undulating mountains (LUM), and great large undulating mountains (GLUM). Their spatial distribution is shown in Figure 3.

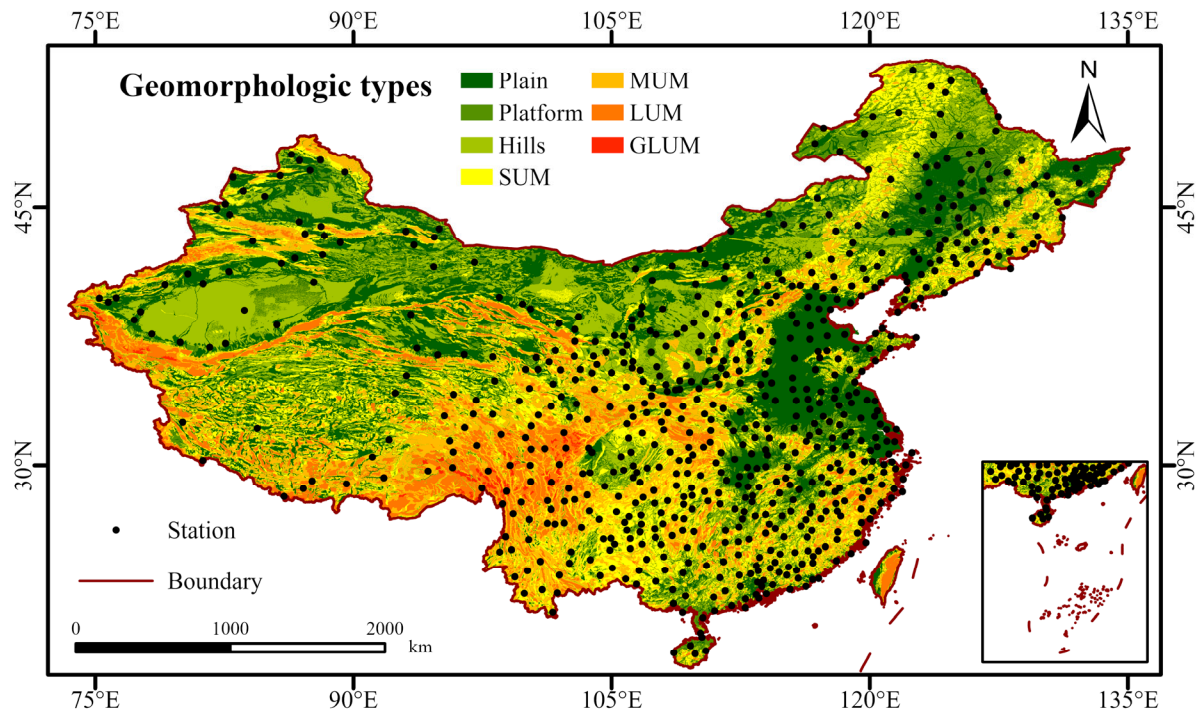


**Figure 3.** Spatial distribution of different geomorphologic types in the studied area.

### 3. Data and Methodology

#### 3.1. Data

##### 3.1.1. IMERG

The GPM core platform is a joint U.S. and Japanese initiative that provides global microwave-based rain and snow data within 3 h and microwave infrared-based rain and snow data within 0.5 h, with coverage extending to the Antarctic and Arctic Circles. This product combines dual-frequency precipitation radar with microwave and infrared observation data, greatly improving the detection capability of weak ( $<0.5$  mm/h) and solid precipitation [18]. As one of the mainstream precipitation datasets in the GPM era, the IMERG product can be divided into IMERG\_Early, IMERG\_Late, and IMERG\_Final. This study selected IMERG\_Final as the research dataset, which was sourced from the NASA official website (<https://disc.gsfc.nasa.gov/> (accessed on 26 May 2022)). The spatial resolution of this product was  $0.1^\circ \times 0.1^\circ$  with daily time resolution. In this study, IMERG\_Final is referred to as IMERG.

##### 3.1.2. GSMaP

GSMaP is a high-precision, high temporal and spatial resolution satellite precipitation dataset provided by the Japan Aerospace Exploration Agency (JAXA, Tokyo, Japan). This dataset includes GSMaP\_NRT, GSMaP\_MVK, and GSMaP\_Gauge [14]. This study used the GSMaP\_Gauge version 07 of the precipitation dataset, which has a spatial resolution of  $0.1^\circ \times 0.1^\circ$  and spatial coverage of  $60^\circ\text{N}$ – $60^\circ\text{S}$ . In this study, GSMaP\_Gauge is referred to as GSMaP and it was sourced from <https://sharaku.eorc.jaxa.jp/GSMaP/index.htm> (accessed on 7 January 2022).

### 3.1.3. ERA5

ERA5, funded by the European Union and operated by ECMWF, is the latest generation of reanalysis data created by the Copernicus Climate Change Service (C3S). ERA5-Land was produced by replaying the terrestrial component of ERA5 climate reanalysis, covering the period from 1981 to the present [18]. In this study, the daily precipitation dataset from ERA5-Land (hereinafter referred to as ERA5) was selected for the period 2001–2020, a total of 20 years. The spatial resolution was  $0.1^\circ \times 0.1^\circ$ , and it was sourced from <https://www.ecmwf.int/> (accessed on 7 April 2023).

### 3.1.4. Other Data

This study collected daily precipitation data from 699 ground meteorological observation stations in the Chinese region from 2001 to 2020. The data were sourced from the China Meteorological Science Data Center (<http://data.cma.cn/> (accessed on 9 April 2023)). The spatial distribution of the ground observation stations is shown in Figures 1–3.

The basin and agricultural zoning data and geomorphologic type data used in this study were all sourced from the Resource and Environment Science and Data Center (<https://www.resdc.cn/> (accessed on 15 April 2023)). The specific spatial distribution of the basin zones is shown in Figure 1, that of the agricultural zones is shown in Figure 2, and that of the geomorphologic types is shown in Figure 3. The specific information of all the data used in this study is shown in Table 1.

**Table 1.** Data and their sources.

Data	Spatial Resolution	Temporal Resolution	Spatial Coverage	Period	Research Timeline	Source
IMERG_Final	$0.1^\circ \times 0.1^\circ$	Daily	Global	2000–2021	2001–2020	<a href="https://disc.gsfc.nasa.gov/">https://disc.gsfc.nasa.gov/</a> (accessed on 26 May 2022)
GSMaP_Gauge		Daily	60°N–60°S	2000–present		<a href="https://sharaku.eorc.jaxa.jp/GSMaP/index.htm">https://sharaku.eorc.jaxa.jp/GSMaP/index.htm</a> (accessed on 7 January 2022)
ERA5_Land		Hourly	Global (land)	1950–present		<a href="https://www.ecmwf.int/">https://www.ecmwf.int/</a> (accessed on 7 April 2023)
Station precipitation data	—	Daily	—	1951–present		<a href="https://data.cma.cn/">https://data.cma.cn/</a> (accessed on 9 April 2023)
Basin zoning data	—	—	China	—	—	<a href="https://www.resdc.cn/">https://www.resdc.cn/</a> (accessed on 15 April 2023)
Agricultural zoning data	—	—	China	—	—	
Geomorphologic types data	—	—	China	—	—	

### 3.2. Methodology

To comprehensively assess the applicability of the three precipitation products, IMERG, GSMaP, and ERA5, in the Chinese region, this study selected 10 common indicators, namely: correlation coefficient (CC), root mean square error (RMSE), relative bias (BIAS), mean absolute error (MAE), Kling–Gupta efficiency (KGE), probability of detection (POD), false alarm ratio (FAR), accuracy (ACC), critical success index (CSI), and equitable threat score (ETS) [9,34,53]. Among them, five statistical indicators, including CC, RMSE, BIAS, MAE, and KGE, were used to evaluate the accuracy error between precipitation product data and ground observation station data. The other five classification indicators, including POD, FAR, ACC, CSI, and ETS, were used to evaluate the precipitation event detection capability of the precipitation products. The specific information is shown in Table 2.

**Table 2.** Information about ten evaluation indicators used in this study.

Statistical Metric	Equation	Perfect Value	Value Range
Correlation Coefficient (CC)	$CC = \frac{\sum_{i=1}^n (G_i - G)(S_i - S)}{\sqrt{\sum_{i=1}^n (G_i - G)^2} \times \sqrt{\sum_{i=1}^n (S_i - S)^2}}$	1	[−1, 1]
Root Mean Square Error (RMSE)	$RMSE = \sqrt{\frac{1}{n} \sum_{i=1}^n (S_i - G_i)^2}$	0	[0, +∞)
Relative Bias (BIAS)	$BIAS = \frac{\sum_{i=1}^n (S_i - G_i)}{\sum_{i=1}^n G_i} \times 100\%$	0	(−∞, +∞)
Mean Absolute Error (MAE)	$MAE = \frac{1}{n} \sum_{i=1}^n  S_i - G_i $	0	[0, +∞)
Kling–Gupta Efficiency (KGE)	$KGE = 1 - \sqrt{(1 - CC)^2 + \left(1 - \frac{S}{G}\right)^2 + \left(1 - \frac{S_S}{S_G}\right)^2}$	1	(−∞, 1]
Probability of Detection (POD)	$POD = \frac{H}{H+F+M}$	1	[0, 1]
False Alarm Ratio (FAR)	$FAR = \frac{H+F}{H+F+Z}$	0	[0, 1]
Accuracy (ACC)	$ACC = \frac{H+Z}{H+F+M+Z}$	1	[0, 1]
Critical Success Index (CSI)	$CSI = \frac{H}{H+F+M}$	1	[0, 1]
Equitable Threat Score (ETS)	$ETS = \frac{H - \frac{(H+F)(H+M)}{H+F+M+Z}}{H+F+M - \frac{(H+F)(H+M)}{H+F+M+Z}}$	1	[0, 1]

In this table,  $S$  and  $G$  represent the precipitation observed by the gridded precipitation products and ground observation stations, respectively, and  $n$  is the sample size.  $G$  and  $S_G$  are the mean and standard deviation of the precipitation observed at the ground observation stations, respectively.  $S$  and  $S_S$  are the mean and standard deviation of the precipitation monitored by the gridded precipitation products, respectively.  $H$  is the number of precipitation events monitored simultaneously by the precipitation products and ground observation stations.  $F$  represents the number of precipitation events that were monitored by the precipitation products but not by the ground observation stations.  $M$  is the number of precipitation events monitored by the ground observation stations but not by the precipitation products.  $Z$  represents the number of non-precipitation events detected simultaneously by both the precipitation products and ground observation stations.

## 4. Results

### 4.1. Time Scale

#### 4.1.1. Annual Time Scale

We analyzed the applicability of the three precipitation products, IMERG, GSMaP, and ERA5, based on the annual precipitation data accumulated from 699 ground observation stations in the study area from 2001 to 2020 as the “true values”. According to the results shown in Figure 4, the applicability of the precipitation products was best in 2006 during the 20 years from 2001 to 2020, and the IMERG satellite precipitation product had higher accuracy than the GSMaP and ERA5 precipitation products, with a CC of 0.98, RMSE of 137.07 mm/year, BIAS of 4.84%, MAE of 97.57 mm/year, and KGE of 0.95. On the other hand, the overall accuracy of the precipitation products was lowest in 2003, when the GSMaP satellite precipitation product had lower accuracy than the IMERG and ERA5 precipitation products, with a CC of 0.54, RMSE of 387.15 mm/year, BIAS of −7.32%, MAE of 304.89 mm/year, and KGE of 0.45. Overall, the applicability of the precipitation products in the first decade (2001–2010) was better than that in the second decade (2011–2020). Within the second decade, the applicability of the three precipitation products during the four years of 2017–2020 was worse than during 2011–2016. Within these four years of 2017–2020, the least applicable precipitation product was the GSMaP satellite precipitation product in 2017, with a CC of 0.65, RMSE of 464.97 mm/year, BIAS of 19.92%, MAE of 375.89 mm/year, and KGE of 0.54.

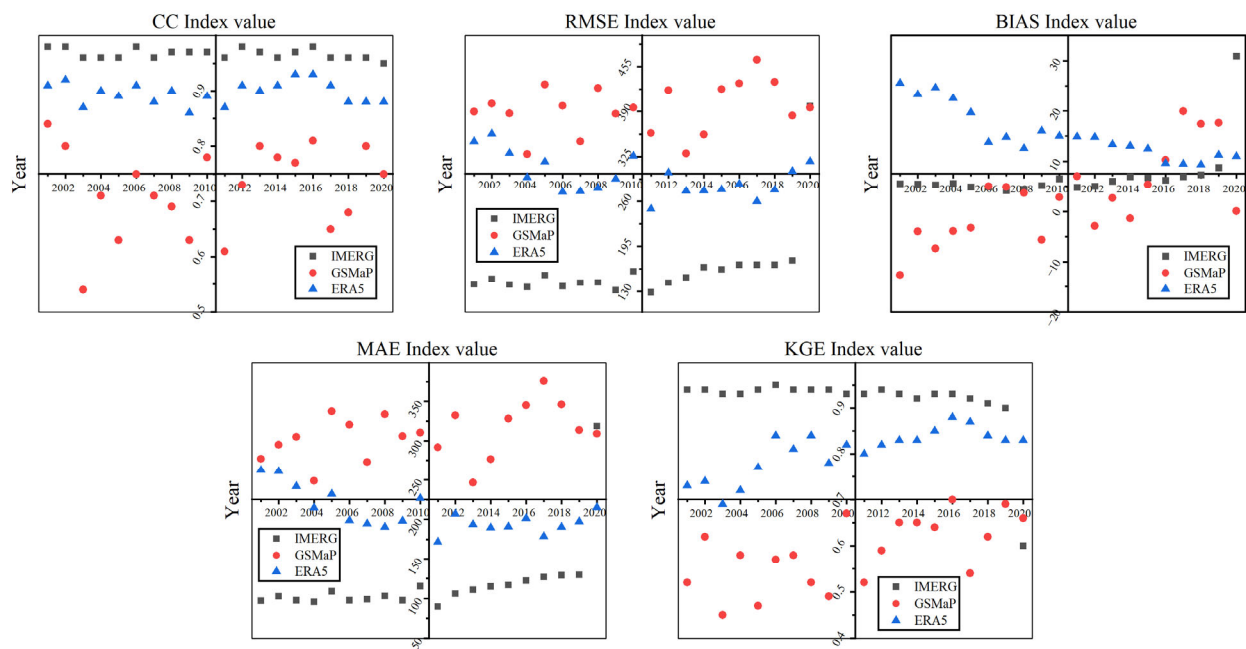


**Figure 4.** Statistical indicator results of the three precipitation products (IMERG, GSMaP, and ERA5) and ground observation station data from 2001 to 2020. The units of RMSE and MAE are both in mm/year, and that of BIAS is in %.

Among the three precipitation products, IMERG, GSMaP, and ERA5, the best performance with the annual precipitation data from the ground observation stations was achieved by the IMERG precipitation product, where the CC was basically 0.97, RMSE was basically 140 mm/year, BIAS was basically around 5.5%, MAE was basically 110 mm/year, and KGE was basically greater than 0.90. The ERA5 precipitation product showed the second best fit, where the CC was basically 0.89, RMSE was basically 280 mm/year, BIAS was basically around 16%, MAE was basically 200 mm/year, and KGE was basically greater than 0.82. The worst performing product was the GSMaP precipitation product, where the CC was basically 0.72, RMSE was basically 390 mm/year, BIAS was basically around 7.24%, MAE was basically 300 mm/year, and KGE was basically greater than 0.60.

By analyzing the various indicators of the three precipitation products, IMERG, GSMaP, and ERA5, in the annual time dimension in the last two decades, we found that the IMERG satellite precipitation product had the best applicability in the Chinese region.

#### 4.1.2. Monthly Time Scale

We analyzed the applicability of IMERG, GSMaP, and ERA5 monthly precipitation data using the monthly average precipitation data accumulated from all ground observation stations in the study area from 2001 to 2020 as the “true values”. According to the results shown in Figure 5, except for October, the slope  $K$  of the linear regression between the IMERG precipitation product and ground observation station data was less than 1 for the other eleven months, indicating that IMERG precipitation data were generally larger than ground observation station data during these months. The best fit was observed in April, with a CC between IMERG satellite precipitation data and ground observation station data of 0.99, RMSE of 10.64 mm/month, BIAS of 7.12%, MAE of 7.44 mm/month, and KGE of 0.92. Good fits were also observed in months with higher precipitation (June to August), with a CC of above 0.95, RMSE of greater than 20 mm/month, BIAS of around 7.4%, MAE of around 17.00 mm/month, and KGE of around 0.91.

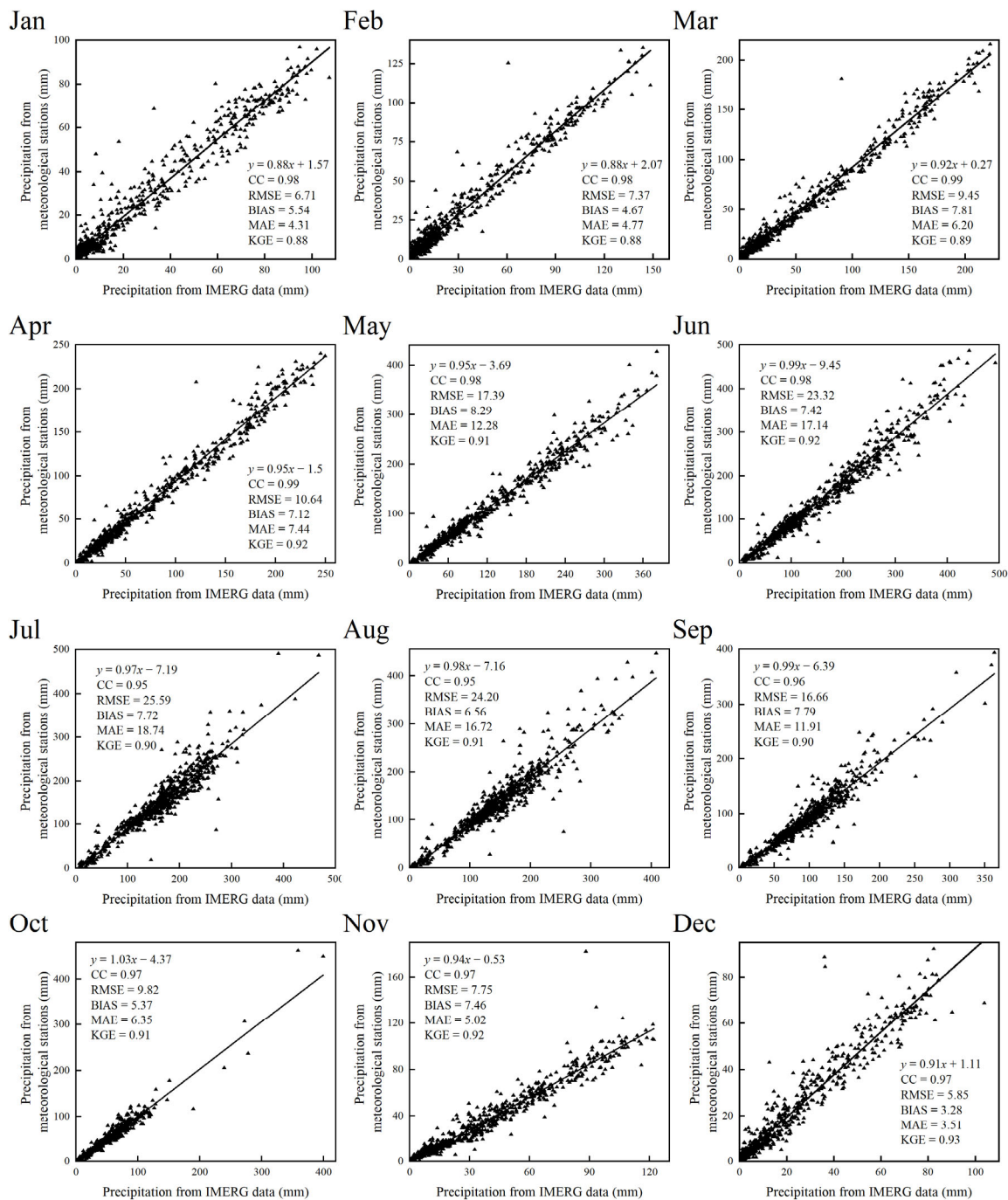


**Figure 5.** Linear relationship between IMERG data and ground observation station precipitation data in 12 months. The units of RMSE and MAE are both in mm/month, and that of BIAS is in %.

The linear relationship between the GSMaP precipitation product and ground observation station precipitation data in the 12 months is shown in Figure 6. It could be observed that the slope  $K$  of the linear regression was greater than 1 for the months of May–June and August, indicating that GSMaP precipitation data were lower than ground observation station precipitation data during these months. The best fit was observed in June, with a CC between GSMaP satellite precipitation data and ground observation station data of 0.85, RMSE of 55.34 mm/month, BIAS of 0.81%, MAE of 44.28 mm/month, and KGE of 0.70. The poorest fit was observed in October, where the CC between GSMaP satellite precipitation data and ground observation station data was 0.53, RMSE was 34.79 mm/month, BIAS was 13.15%, MAE was 26.48 mm/month, and KGE was 0.47. Relative to the months with

less precipitation, the months with more precipitation (May to August) exhibited better fits, with a CC of above 0.78, RMSE of around 50 mm/month, BIAS of around 10%, MAE of around 40 mm/month, and KGE of around 0.65.

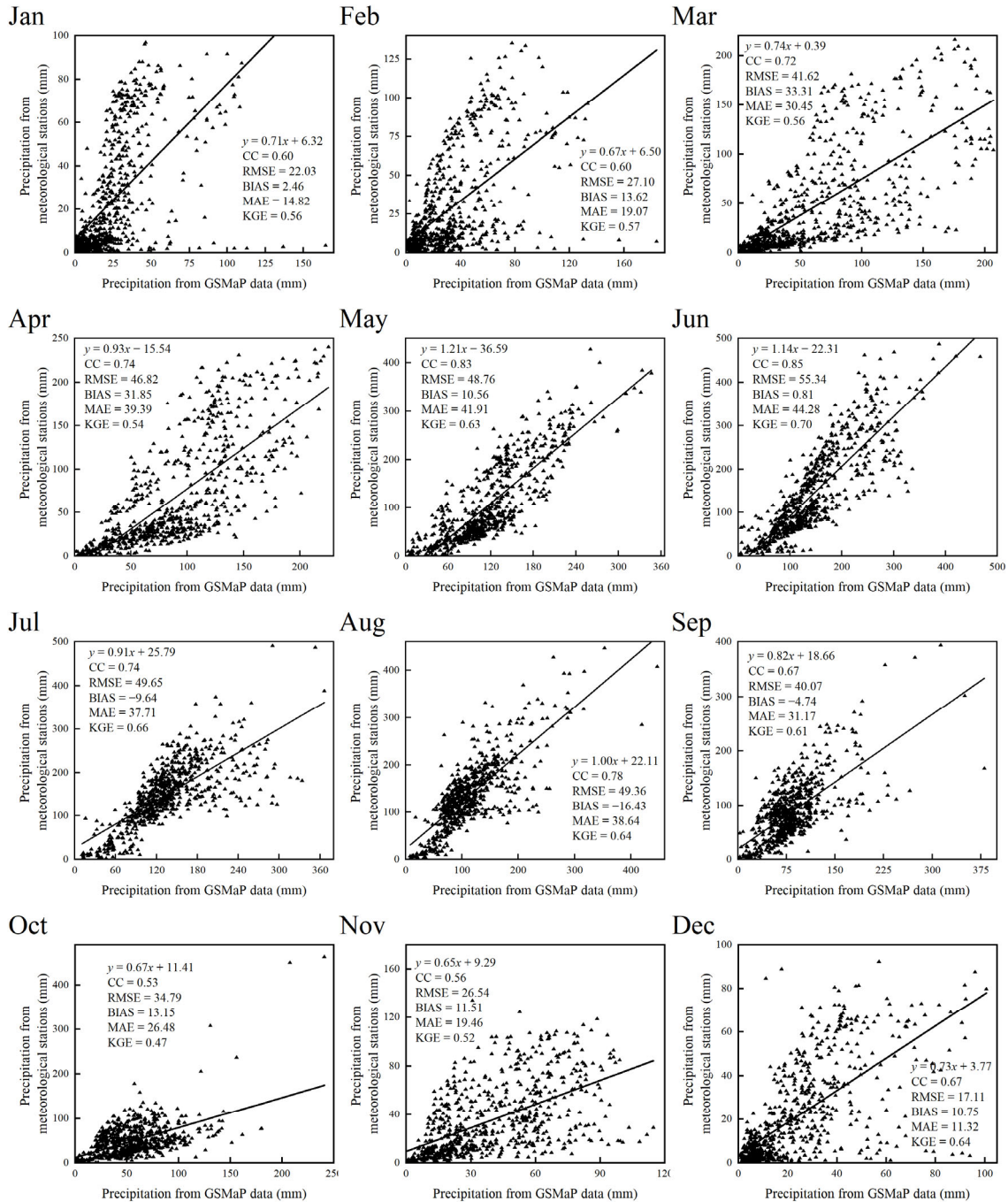


**Figure 6.** Linear relationship between GSMaP data and ground observation station precipitation data in 12 months. The units of RMSE and MAE are both in mm/month, and that of BIAS is in %.

The linear relationship between the ERA5 precipitation product and ground observation station precipitation data for 12 months is shown in Figure 7. The analysis showed that the slope  $K$  of the linear regression was less than 1 for all months, indicating that ERA5 precipitation data were generally larger than precipitation data from the ground observation stations in all months. The best fit was observed in May, with a CC between ERA5 precipitation data and ground observation station data of 0.94, RMSE of 33.92 mm/month,

BIAS of 14.03%, MAE of 22.17 mm/month, and KGE of 0.84. The poorest fit was observed in October, where the CC between GSMaP satellite precipitation data and ground observation station data was 0.84, RMSE was 23.20 mm/month, BIAS was 18.74%, MAE was 13.67 mm/month, and KGE was 0.75.

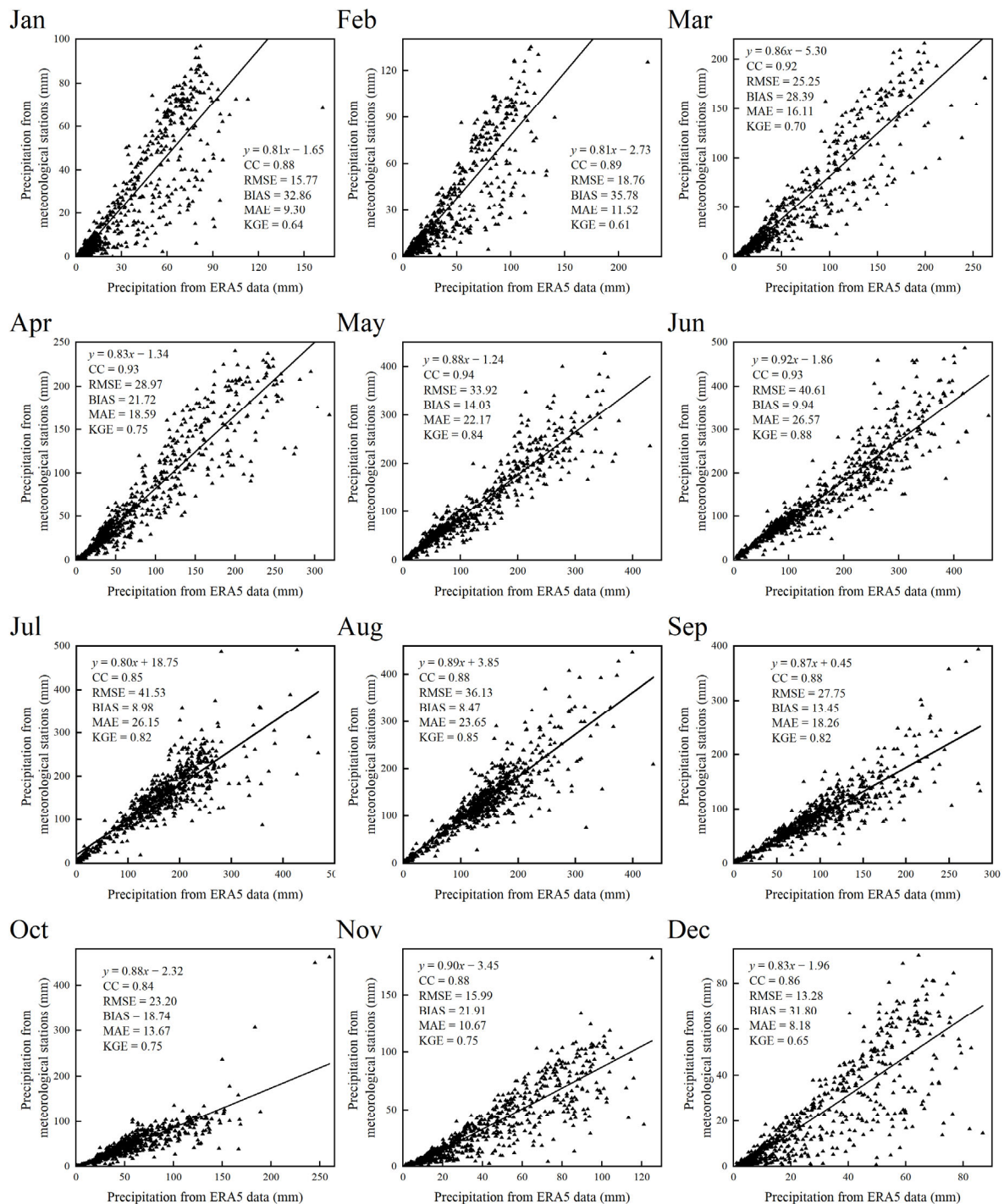


**Figure 7.** Linear relationship between ERA5 data and ground observation station precipitation data in 12 months. The units of RMSE and MAE are both in mm/month, and that of BIAS is in %.

Based on the convergence analysis of the 12 months, the fit between the IMERG precipitation product and ground observation station data was better than that of the other two precipitation products (GSMaP and ERA5), especially during months with higher

precipitation (May to September). For this reason, on a monthly time scale, the IMERG satellite precipitation product exhibited the best applicability in the Chinese region.

#### 4.1.3. Daily Time Scale

We analyzed the applicability of three precipitation products, namely IMERG, GSMaP, and ERA5, by comparing them with the “true value” daily precipitation data from all ground observation stations in the study area. According to the results shown in Figure 8, it could be seen that the CC value between the GSMaP precipitation product and ground observation precipitation station data was the lowest, while the IMERG and ERA5 precipitation products had similar CC values throughout the year. From January to June and September to December, the RMSE values between the GSMaP precipitation product and ground observation precipitation station data were significantly larger than those for the IMERG and ERA5 precipitation products. In July and August, the RMSE values for the IMERG, GSMaP, and ERA5 precipitation products were similar throughout the year. In May–June and September, the ERA5 precipitation product had significantly lower RMSE values than the IMERG precipitation product. Regarding the BIAS indicator, the three precipitation products showed larger fluctuations from January to April and October to December. From May to early-to-mid June, the BIAS values for all three precipitation products were similar. From mid-to-late June to September, IMERG and ERA5 data performed better than GSMaP data, while IMERG and ERA5 data had similar BIAS values. The changes in MAE for the three precipitation products were similar to those in RMSE and are not described in detail. In terms of KGE, all three precipitation products showed larger fluctuations from January to April and October to December. From May to September, the KGE values for all three precipitation products were similar, but IMERG and ERA5 had slightly higher KGE values than GSMaP. The POD values of ERA5 data were significantly higher than those of IMERG and GSMaP data, where IMERG data had slightly higher POD values than GSMaP data. For the FAR indicator, GSMaP data performed better than both IMERG and ERA5 data, especially from June to September, while IMERG data performed slightly better than ERA5 data. In terms of the ACC indicator, the ACC values of IMERG data were lower than those of the other two products from mid-to-late April to early-mid June. From February to April and from July to September, GSMaP data performed significantly better than the other two products, while ERA5 data had the lowest ACC values. In terms of the CSI indicator, ERA5 data performed significantly better than the other two products from January to June and September to December, while in July and August, GSMaP data slightly outperformed the other two products, with ERA5 data performing the worst. In terms of the ETS indicator, from mid-to-late June to mid-to-late September, ERA5 data had the lowest ETS values, while GSMaP data had the highest ETS values. In the other months, ERA5 data had the highest ETS values, with IMERG data having the lowest ETS values in April–May and October.

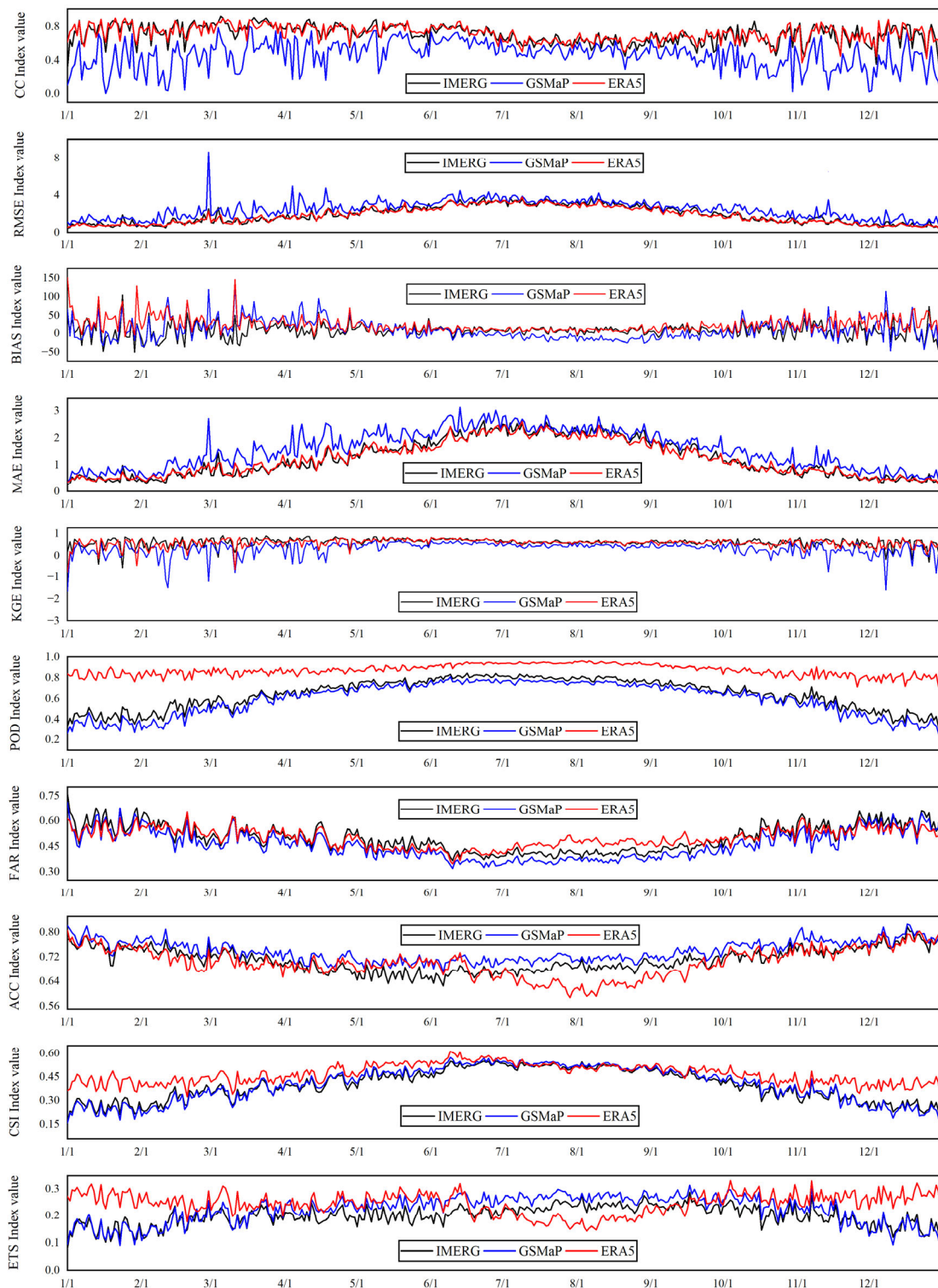


**Figure 8.** Evaluation index results of daily precipitation data for the three products (IMERG, GSMaP, and ERA5). The units of RMSE and MAE are both in mm/day, and that of BIAS is in %.

Based on the comprehensive statistical analysis, it could be concluded that ERA5 and IMERG data exhibited better applicability than GSMaP data, with ERA5 data slightly outperforming IMERG data. In terms of categorical indicators analysis, GSMaP and IMERG data demonstrated better applicability than ERA5 data, with GSMaP data slightly outperforming IMERG data. Considering both statistical and categorical indicators, we believe that IMERG data exhibited the best applicability in the Chinese region.

#### 4.2. Spatial Dimension

This study also analyzed the applicability of the three gridded precipitation products in terms of spatial dimension, and the spatial distribution of the evaluation indicators is shown in Figures 9 and 10. Overall, the applicability of the three gridded precipitation products gradually decreased along the southeast–northwest direction. To better evaluate the applicability of the three precipitation products in the regional spatial dimension, we further assessed their accuracy in terms of basins, agriculture, and geomorphology.

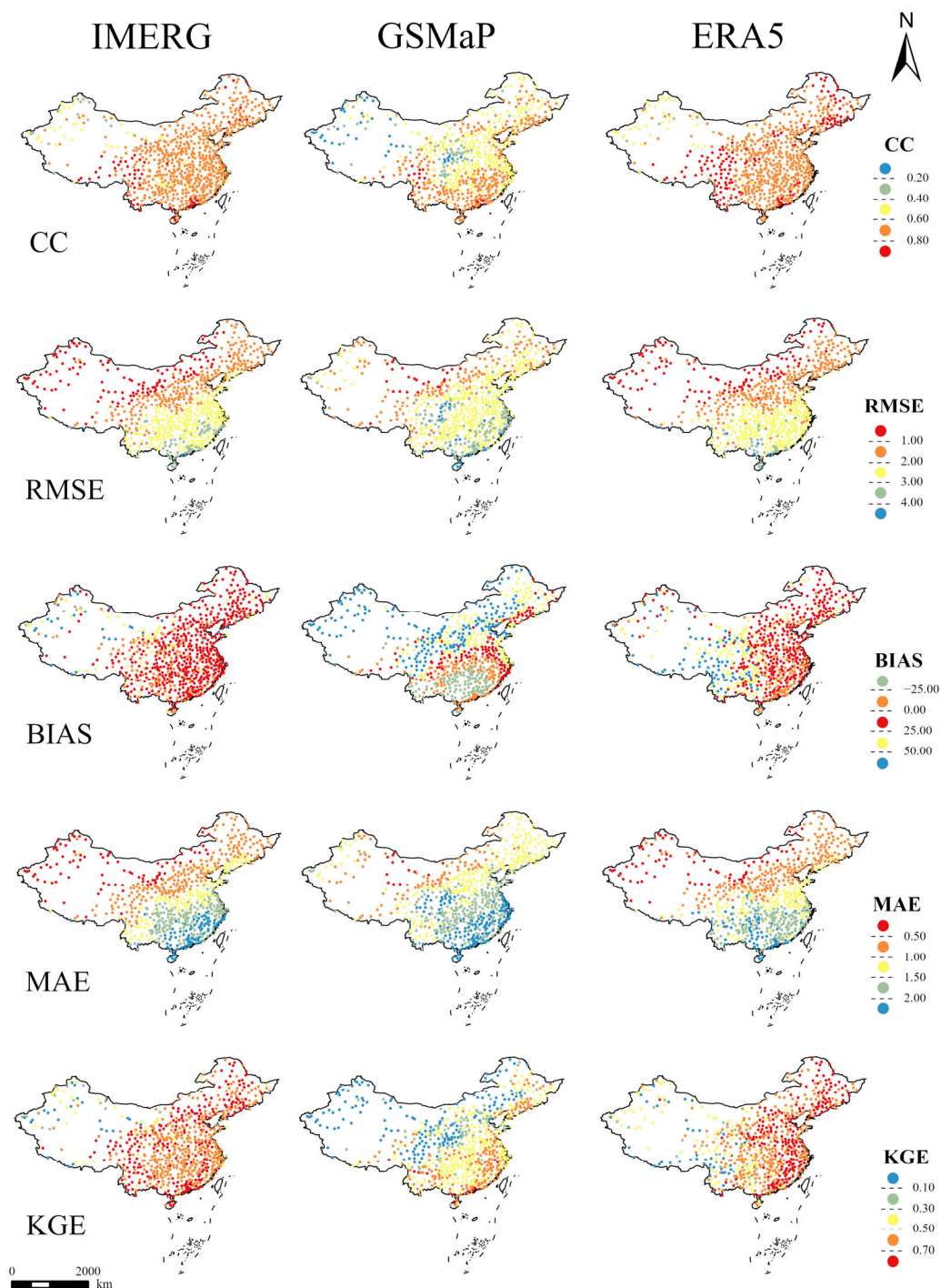


**Figure 9.** Spatial distribution of statistical indicators of three precipitation products (IMERG, GSMaP, and ERA5) at different stations. The units of RMSE and MAE are both in mm/day, and that of BIAS is in %.

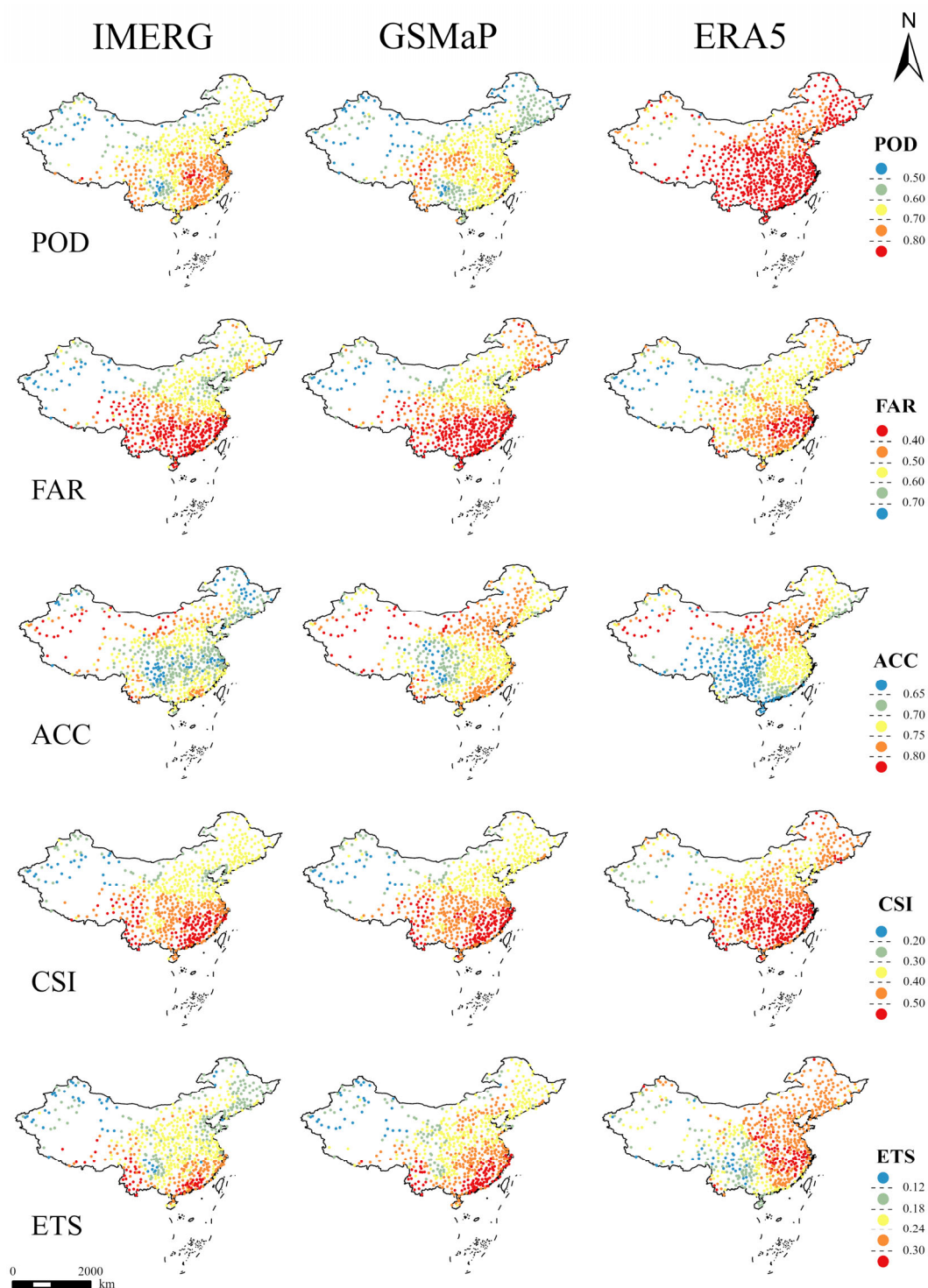


**Figure 10.** Spatial distribution of classification indicators of three precipitation products (IMERG, GSMaP, and ERA5) at different stations.

#### 4.2.1. Basin Zoning

We analyzed the applicability of three precipitation products, namely IMERG, GSMaP, and ERA5, in the nine basin zones using the “true value” daily precipitation data from all ground observation stations in the study area. The number of ground observation stations in Yangtze RB accounted for 28.77% of the total stations. The ground observation stations in S&L RB, Yellow RB, and Pearl RB each accounted for approximately 12% of the total

stations. Southeast B, Hai RB, and Southwest B had the lowest proportions of ground observation stations, accounting for only around 5% of the total stations.

According to the results shown in Figure 11, among the nine basin zones, the CC values between the three precipitation products and ground observation station precipitation data were generally around 0.75 in eight basin zones, except for Continental B where the CC value was relatively poor. Among them, Southwest B had the highest CC value. The basin with the most CC anomalies was Yangtze RB when the GSMaP precipitation product was used. In terms of RMSE, the lowest values were observed in Continental B, especially when using the IMERG and ERA5 precipitation products, at only about 0.5 mm/day. The highest RMSE values were found in Pearl RB, reaching around 3 mm/day. The basin with the most RMSE anomalous values remained Yangtze RB. Regarding the BIAS indicator, the best distribution of values was observed in Hu RB, with BIAS values closest to 0. The worst distribution of BIAS values was found in Continental B, which also had many anomalous values. The distribution of MAE values among the nine basin zones was similar to that of RMSE values. Compared to the RMSE index, Yangtze RB had fewer anomalous values in the MAE index. For the KGE indicator, Southeast B had the best distribution of values, while Continental B had the worst distribution.

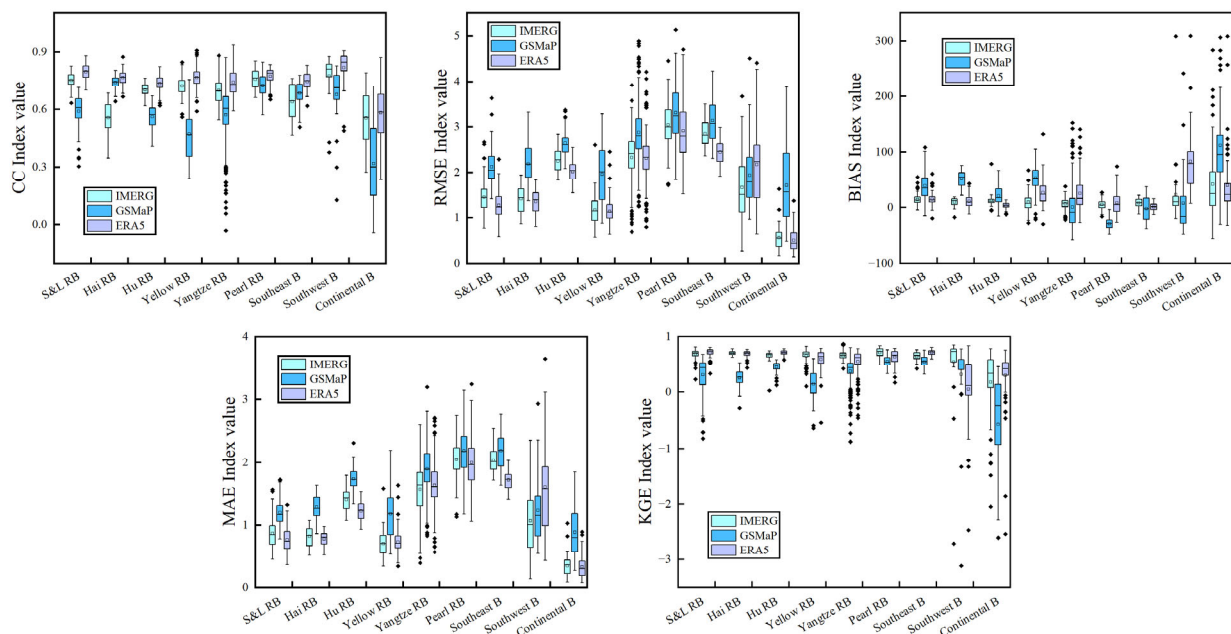


**Figure 11.** Statistical indicator results of three precipitation products (IMERG, GSMaP, and ERA5) in different basin zones. The units of RMSE and MAE are both in mm/day, and that of BIAS is in %.

From the results shown in Figure 12, we can observe that, in terms of the POD index, the best numerical distribution was found in Southwest B, especially when using the ERA5 precipitation product, with POD values as high as about 0.98. The poorest distribution of POD values was found in Continental B, and Yangtze RB had more anomalous POD values. As for the FAR indicator, Pearl RB and Southeast B showed consistent numerical distributions, with a FAR value of around 0.3 when using the GSMaP precipitation product, which was better than that of the other seven basin zones. The poorest distribution of FAR values was found in Continental B, with Yangtze RB and Southeast B having more anomalous FAR values. In terms of the ACC indicator, Continental B significantly outperformed the other eight basin zones, while Yangtze RB exhibited the poorest numerical distribution. Regarding the CSI indicator, Southeast B showed the best numerical distribution, while Continental B exhibited the poorest numerical distribution. Yangtze RB had more anomalous CSI values. Finally, for the ETS indicator, Pearl RB and Southwest B exhibited

consistent numerical distributions, which were better than those of the other seven basin zones, while Continental B showed the poorest numerical distribution.

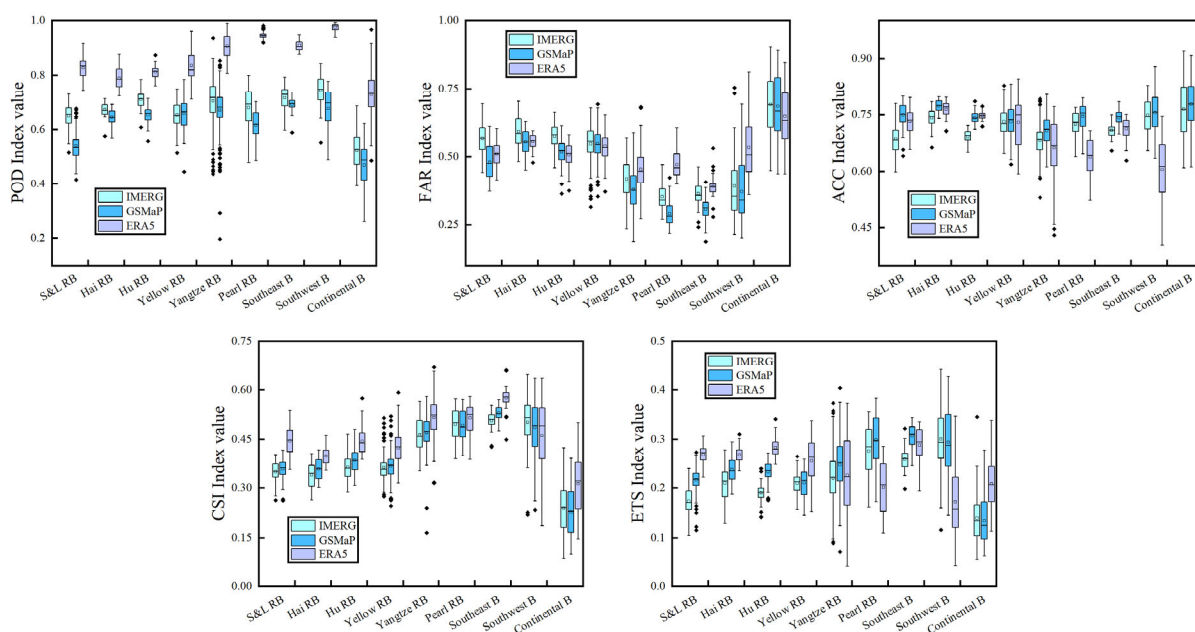


**Figure 12.** Classification indicator results of three precipitation products (IMERG, GSMaP, and ERA5) in different basin zones.

Based on the above, among the nine basin zones, the best overall distribution of various indicators was observed in Southeast B, followed by Southwest B, while the least favorable distribution was found in Continental B. Additionally, we believe that the ERA5 precipitation product was most applicable for Southeast B and Continental B, while the IMERG precipitation product was most applicable for Southwest B. For the other basin zones, the choice of appropriate gridded precipitation product should be based on individual needs.

#### 4.2.2. Agricultural Zoning

The Chinese region mainly included nine agricultural zones, among which the number of ground observation stations in the MLYP agricultural zone accounted for 20.70% of the total stations, followed by NASR, which accounted for 16.76% of the total stations. The three agricultural zones of SC, LP, and HHHP each accounted for about 8% of the total stations. QTP had the fewest stations, accounting for only 6.12% of the total stations.

From the results shown in Figure 13, it could be observed that the QTP agricultural zone had the best numerical distribution for the CC index, while the CC numerical distribution when using the GSMaP precipitation product was extremely poor, and there were more anomalous CC values in this agricultural zone. The NASR agricultural zone had the overall worst numerical distribution of the CC index. For the RMSE index, NASR had the best numerical distribution, while SC had the worst CC numerical distribution. For the BIAS index, SC had the best numerical distribution. NASR had the worst numerical distribution of BIAS values, especially when using the GSMaP precipitation product, and it had the highest number of anomalous BIAS values. The numerical distribution of the MAE index was consistent with that of the RMSE index. In terms of the KGE indicator, SC had the best numerical distribution, especially when using IMERG precipitation data. NASR had the worst numerical distribution of KGE values and the highest number of anomalous KGE values.

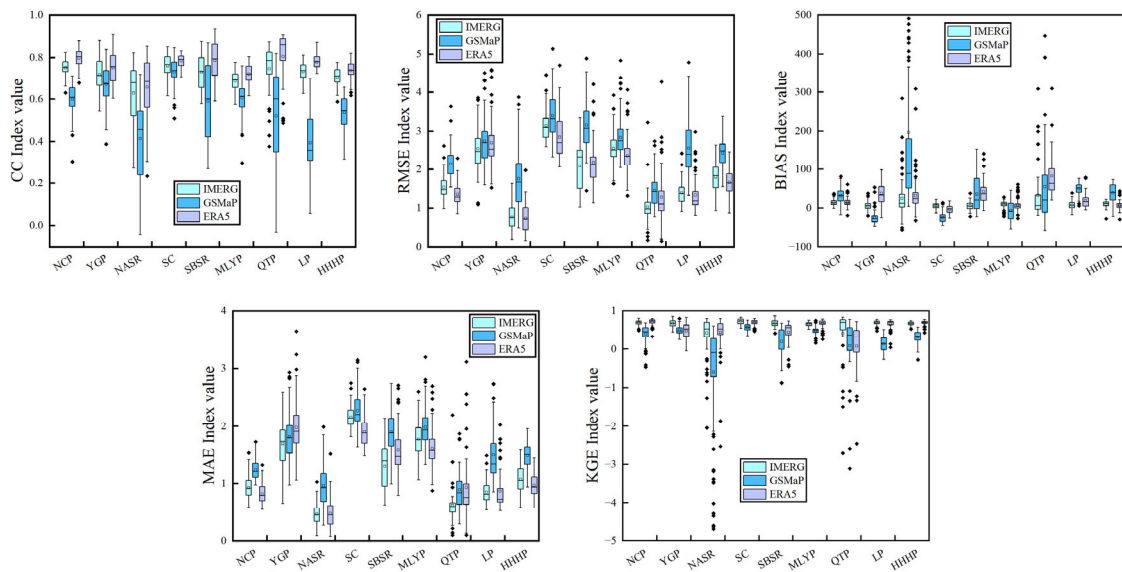


**Figure 13.** Statistical indicator results of three precipitation products (IMERG, GSMaP, and ERA5) in different agricultural zones. The units of RMSE and MAE are both in mm/day, and that of BIAS is in %.

From the analysis shown in Figure 14, it could be observed that the SC agricultural zone had the best distribution of values in terms of the POD index, but it also had a higher number of anomalous values. On the other hand, NASR had the worst distribution of values for the POD index. In terms of the FAR index, SC had the best distribution of values, while NASR had the worst distribution. For the ACC index, NASR had the best distribution of values, and the three precipitation products performed similarly. SBSR had the worst distribution of values for the ACC index. Regarding the CSI index, SC had the best distribution of values, while NASR had the worst distribution. In terms of the ETS index, SC had the best distribution of values, especially when using the GSMaP precipitation product. NASR had the worst distribution of values for the ETS index.

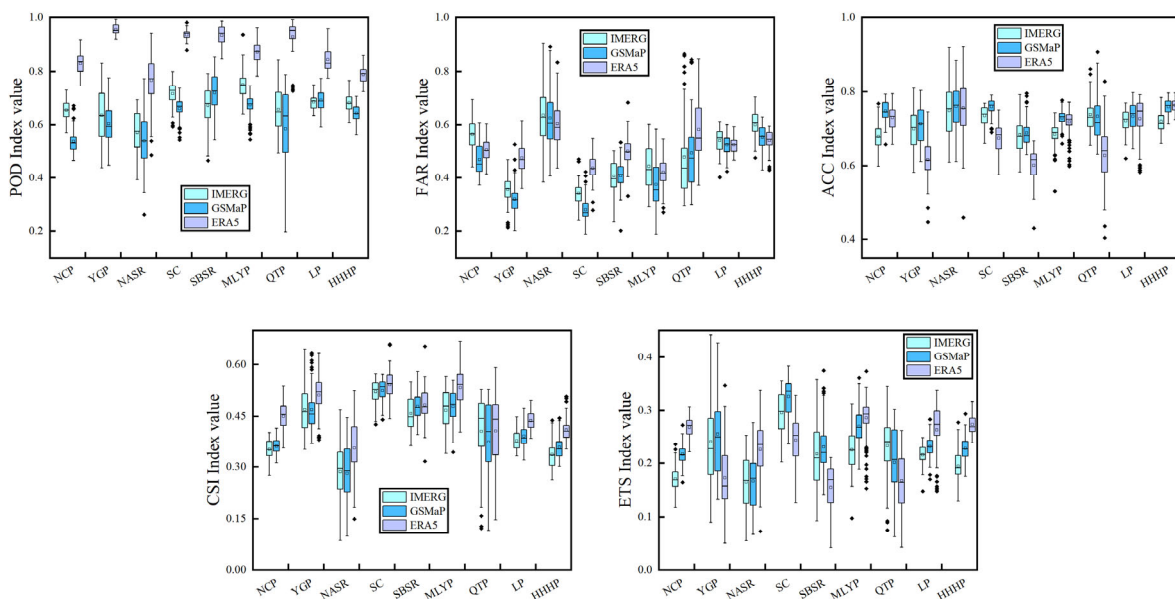


**Figure 14.** Classification indicator results of three precipitation products (IMERG, GSMaP, and ERA5) in different agricultural zones.

In summary, among the nine agricultural zones, the overall best distribution of values was observed in the SC agricultural zone, while the worst distribution was found in NASR. The IMERG precipitation product was most applicable for SC, while the ERA5 precipitation product was most applicable for NASR. For the other agricultural zones, the choice of the most appropriate precipitation product should be based on the specific requirements.

#### 4.2.3. Geomorphologic Types

The Chinese region mainly included seven geomorphologic types, with the plains zone accounting for 55.16% of the total ground observation stations, followed by the platforms zone accounting for 20.28% of the total stations, hills accounting for 11.03% of the total stations, and mountains accounting for 13.52% of the total stations. Among them, SUM accounted for the highest proportion within the mountainous zone, reaching 6.23%.

According to the analysis of the daily dimension error indices of the three precipitation products under different geomorphologic types, as shown in Figure 15, the CC values in LUM were higher than those of the other six geomorphologic types, especially when ERA5 data were used. GLUM had the lowest CC values, followed by the plains zone, where the most anomalous CC values occurred. In terms of the RMSE index, the plains zone had the best distribution of values. GLUM had the worst distribution, with increasing undulation leading to higher RMSE values. In terms of the BIAS index, platforms had the best distribution of values, especially when using IMERG data. MUM had the worst distribution of BIAS values. The plains zone had the most anomalous BIAS values. In terms of the MAE index, the plains zone had the best distribution of values. In terms of the KGE index, the platforms zone had the best distribution of values, especially when using IMERG data. The MUM zone had the worst distribution of KGE values. The plains and platforms zones had the most anomalous KGE values.

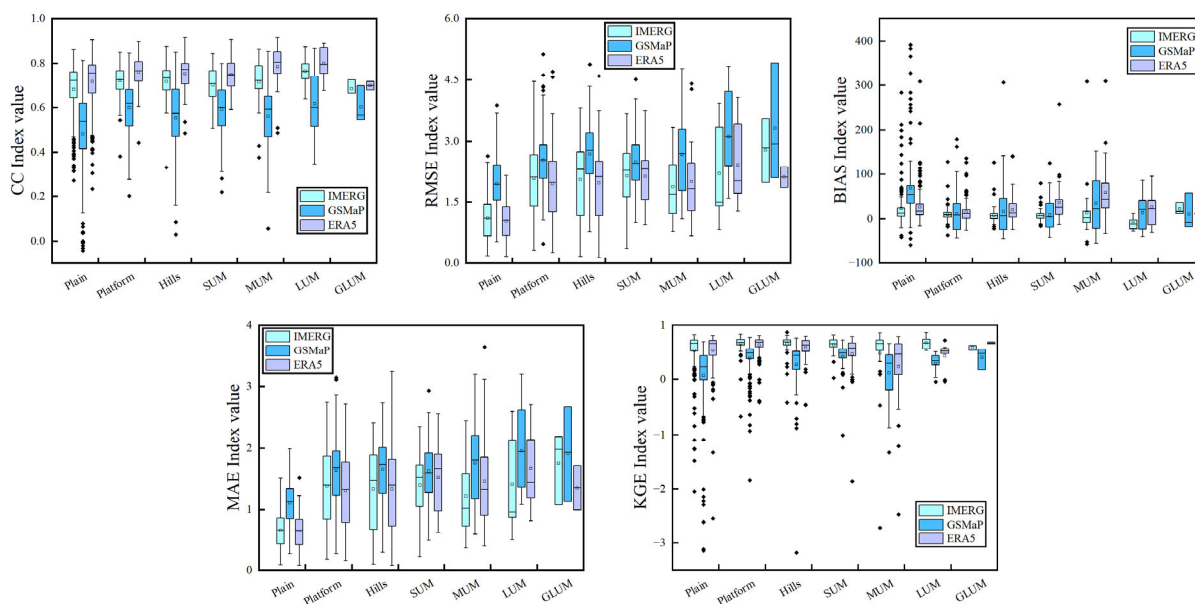


**Figure 15.** Statistical indicator results of three precipitation products (IMERG, GSMaP, and ERA5) in different geomorphologic types. The units of RMSE and MAE are both in mm/day, and that of BIAS is in %.

According to the analysis shown in Figure 16, it could be observed that in terms of the POD indicator, LUM exhibited the best numerical distribution, especially when using ERA5 data. In terms of the FAR indicator, LUM demonstrated the best numerical distribution, especially when using GSMaP data. The plains geomorphologic type exhibited the poorest numerical distribution and had the highest number of anomalous FAR values. In terms of the ACC index, the plains zone showed the best numerical distribution but

also had the highest number of anomalous ACC values. LUM exhibited the best numerical distribution in terms of the CSI indicator. Plains had the poorest numerical distribution and also the highest number of anomalous CSI values. In terms of the ETS indicator, platforms demonstrated the best numerical distribution, surpassing the other six types of geomorphologic types. The plains zone had the poorest numerical distribution and also had the highest number of anomalous ETS values.

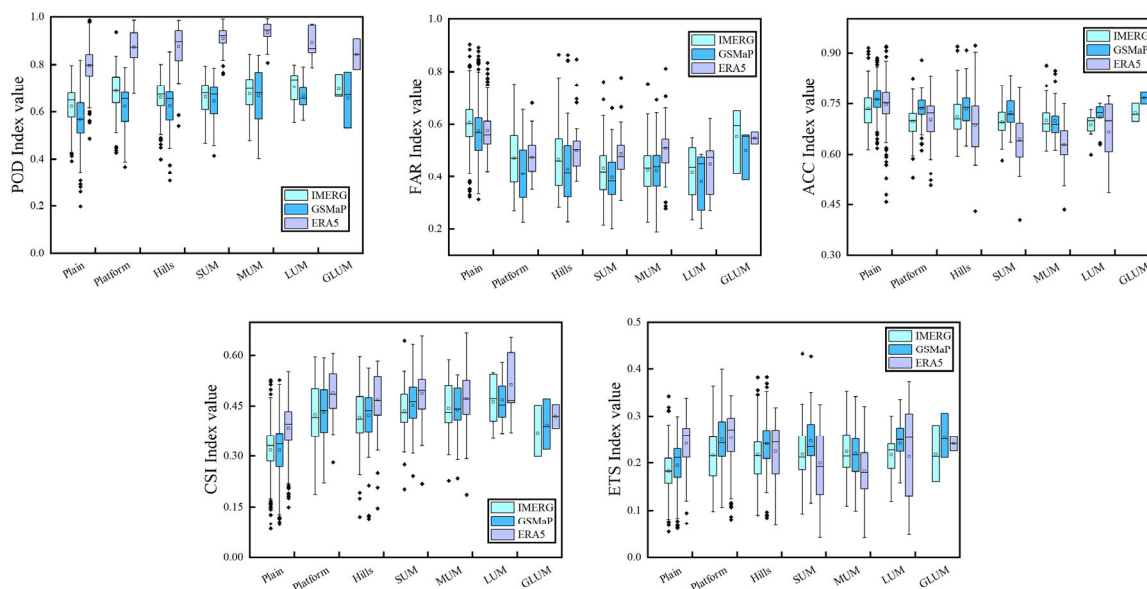


**Figure 16.** Classification indicator results of three precipitation products (IMERG, GSMaP, and ERA5) in different geomorphologic types.

In conclusion, among the seven geomorphologic types, LUM exhibited the best overall numerical distribution, followed by platforms, while MUM and GLUM performed the worst. In terms of the applicability of the precipitation products, the IMERG product performed best in MUM, LUM, and GLUM, while the ERA5 product performed best in platforms. For the other geomorphologic types, the most applicable precipitation product should be selected based on the specific needs.

## 5. Discussion

In this study, we evaluated the applicability of the three precipitation products, IMERG, GSMaP, and ERA5, on different time scales. On the daily time scale, the performance of the three precipitation products was inconsistent for the two different categories of indicators (Figure 8). We analyzed the statistical indicators of daily precipitation data and found that the applicability of the ERA5 precipitation product was better than that of the other two products, especially for the BIAS and KGE indicators, which was inconsistent with the findings of Xu et al. [39]. Considering the global climate change in the last two decades, overall precipitation fluctuations in the study area had increased. Xu et al. [39] focused on the period from 2016 to 2019, while our study focused on the period from 2001 to 2020. The differences in precipitation amounts between these different periods might be the main reason for the inconsistent results. By analyzing the classification indicators of daily precipitation data, we obtained the applicability assessment ranking as GSMaP, IMERG, and ERA5, especially for the FAR, ACC, and ETS indicators, which were more significant in summer months with abundant precipitation, in agreement with the findings of Tang et al. [49]. Considering the two types of indicators together, IEMRG had the best overall applicability on the daily scale, consistent with the findings of Chen et al. [13], Wang et al. [19], and Weng et al. [48]. However, all three precipitation products overestimated the actual precipitation amount, which was also observed by Chen et al. [13], Wang et al. [19],

and Gentilucci et al. [31]. Gentilucci et al. [31] suggested that this was due to the fact that rain gauges at ground observation stations are generally affected by wind, which interacts with the shape of the rain gauge and results in less rainfall falling into the rain gauge. In China, winds are stronger in winter and snow is common, except in a few areas in the south. Although the rain gauges are of the heated type, snow is more likely to be blown away by the wind, reducing the actual snow accumulation and leading to a more pronounced overestimation of precipitation in the winter.

The overall performance of the IMERG precipitation product was significantly better than that of GSMaP and ERA5 in the annual and monthly dimensions, which was consistent with the findings of Xu et al. [39]. The reason for the inconsistent applicability results of the three precipitation products in the daily dimension compared to the annual and monthly dimensions might be that the IMERG precipitation product had the least overall fluctuations in the daily dimension compared with the GSMaP and ERA5 precipitation products, which subsequently improved the applicability of IMERG data when daily precipitation data were accumulated to form annual and monthly precipitation data. Therefore, the applicability of the three precipitation products was proportional to the time scale, with the best applicability on the annual scale, which was consistent with the findings of Lei et al. [47]. By analyzing the statistical indicators of the annual precipitation data, we found that the overall trends in the applicability of the three precipitation products over the 20 years were not consistent. The applicability of GSMaP showed some fluctuations but the overall trend was not significant. On the other hand, the applicability of ERA5 demonstrated an overall increasing trend, which showed that improvement due to gauge adjustment was greater than improvement due to satellite sensors. The frequency of extreme weather has increased in recent years. However, the IMERG precipitation product had poor detection capabilities for such events, which might have led to a decrease in its applicability. Although the overall trend of the applicability of the IMERG precipitation product was decreasing, its applicability remained superior to that of the previous two precipitation products. The CC between the IMERG precipitation product and ground observation station data was basically better than that of the other precipitation products, especially on annual and monthly scales, in agreement with the findings of Chen et al. [13], Wang et al. [19], and Weng et al. [48]. Additionally, the numerical performance of GSMaP precipitation data in terms of the KGE indicator was consistent with the findings of Tang et al. [49], while the study by Tang et al. [49] did not include the IMERG\_Final and ERA5\_Land precipitation products used in our study, and therefore are not discussed here.

We also assessed the applicability of the three precipitation products, IMERG, GSMaP, and ERA5, in different spatial dimensions. In addition, we calculated the spatial distribution of ten indicators for the three precipitation products over the study's entire spatial region (Figures 9 and 10). The results of the spatial analysis based on basin zoning were consistent with those of Lilan Zhang et al. [12], Weng et al. [48], and Tang et al. [49]. Among the nine basin zones, Southeast B exhibited the highest applicability of the precipitation products, while Continental B showed the lowest. Yangtze RB had the highest overall number of anomalous values. The best applicable precipitation product in both Southeast B and Continental B was ERA5.

In addition, we also analyzed the applicability of the three precipitation products in terms of agricultural zoning and geomorphologic type. Among the nine agricultural zones, the best applicability of the precipitation products was found in SC, while the least applicability was observed in NASR. The MLYP agricultural zone had the highest number of anomalous values overall. The IMERG precipitation product had the best applicability in SC, which could be analyzed from the spatial distribution of indicators such as BIAS (Figure 9) and FAR (Figure 10). The ERA5 precipitation product had the best applicability in NASR, which could also be analyzed as shown in Figures 9 and 10, especially for POD, CSI, and ETS. The geomorphologic types differed from the two spatial zoning mentioned above, in that the seven geomorphologic types were not so distinct from each other, and there were significant differences in the number of ground observation stations among the different

geomorphologic types. The best applicability of the precipitation products was found in LUM, followed by platforms, while the worst applicability was found in MUM and GLUM. The plains geomorphologic type had the highest number of anomalous values overall. However, because there were too few ground stations in some individual geomorphologic types, we categorized the seven geomorphologic types into two basic geomorphologic categories: plains and mountains. We found that the applicability of the precipitation products was generally higher in plains than in mountains, with ERA5 precipitation data showing the best applicability in plains and IMERG precipitation data showing the best applicability in mountains. In addition, we found that there were a large number of index anomalous values in individual spatial zones. In the above-mentioned partitions, we should be careful in selecting precipitation products, and the applicability of precipitation products could be evaluated again by refining the spatial dimension. Otherwise, we could consider using the data from ground observation stations directly.

The main reasons for the differences on temporal scales and in spatial dimensions were the differences in precipitation inversion methods and algorithms used by the different precipitation products [1,39]. In this study, the applicability of only two satellite precipitation products and one reanalysis precipitation product was evaluated from the perspective of temporal scales and spatial dimensions, without considering their inversion accuracy in extreme precipitation events. In this study, we also only analyzed the three mainstream gridded precipitation products. In future studies, we will consider multiple precipitation products, such as MERRA and FY series precipitation products. In addition, passive sensors have limitations and imperfect skill in measuring cloud and precipitation properties, especially in certain scenarios with multilayer clouds and warm rain [54]. As precipitation forms in the clouds when water vapor condenses into droplets, Pipunic et al. [55] indicated that estimates of cloud information could affect the quality of the satellite precipitation product. Further improving the performance of precipitation products based on cloud information is a potential and promising future research direction.

## 6. Conclusions

We evaluated the applicability of three gridded precipitation products (IMERG, GSMaP, and ERA5) in the Chinese region on both temporal scales and in spatial dimensions, using ground observation station precipitation data as the “true values”. The main conclusions were as follows: (1) IMERG data had the best applicability in the annual and monthly time scale analyses, with both CC values greater than 0.95 and KGE values greater than 0.90. However, on the daily time scale, the two types of indicators showed different behaviors. The applicability of ERA5 data was better when statistical indicators were analyzed, and the applicability of GSMaP data was better when categorical indicators were analyzed. Considering both statistical and categorical indicators, IMERG data showed the best applicability. (2) The applicability of the three precipitation products gradually decreased along the southeast–northwest direction. ERA5 data demonstrated better applicability in areas with less precipitation and more ground observation stations, while IMERG data showed better applicability in areas with more precipitation and fewer ground observation stations. Specifically, the applicability of ERA5 data was better in northern regions, especially in arid and semi-arid regions. In contrast, the applicability of IMERG data was better in southern and high-altitude regions. (3) The geomorphologic type with the best applicability for the precipitation products was LUM, followed by platforms, while MUM and GLUM had the lowest applicability. Among the two basic geomorphologic categories of plains and mountains, the applicability was overall better in plains than in mountains. In plains, ERA5 data exhibited better applicability, while in mountains, IMERG data showed better applicability. (4) In other different spatial zones, the most applicable gridded precipitation product should be chosen according to the specific requirements. In spatial divisions with more anomalous index values, the spatial dimension should be refined when using precipitation products. The results of this study could provide a reference

for future researchers in geological disasters, hydrometeorology, agricultural cultivation, etc., to select appropriate precipitation products when needed.

**Author Contributions:** Methodology, H.Z. and S.N.; Software, S.N.; Investigation, H.Z. and Q.L.; Resources, M.Z.; Data curation, S.N.; Writing—original draft, H.Z.; Writing—review & editing, D.L.; Visualization, X.T.; Supervision, X.P. All authors have read and agreed to the published version of the manuscript.

**Funding:** This study was supported by the Jiangsu Provincial Marine Science and Technology Innovation Special Project (Grant No. JSZRHYKJ202206 and JSZRHYKJ202001) and the Ecological Environment Monitoring Research Fund of Jiangsu Province (Grant No. 2329).

**Data Availability Statement:** The data download sources used in this paper are shown in Table 1. Due to privacy and ethical concerns, the results data in this paper cannot be made available.

**Acknowledgments:** We thank the editorial team and anonymous reviewers for their efforts to improve this manuscript.

**Conflicts of Interest:** The authors declare no conflict of interest.

## Appendix A

**Table A1.** Summary of applicability studies using gridded precipitation products in China over the last decade.

Source Documents	Research Region	Using Datasets	Research Timeline	Number of Stations	Time Dimension	Spatial Dimension
Qin et al. [36]	China	TRMM-3B42, TRMM-3B42RT, CMORPH, GSMaP	2003–2006	2000	Quarterly, monthly, daily	Administrative zone, topographic zone
Shen et al. [37]	China	CMORPH	2008–2010 (May–September)	30,000	Daily, hourly	Northeast and northwest regions
Yang and Luo [40]	Northwest China	CMORPH, CMORPH, TRMM(3B42,3B43)	2003–2010	76	Annual, monthly, daily	Topographic zone
Tang et al. [38]	Ganjiang River Basin	TMPA3B42V7, 3B42RT, GPM IMERG	May–September 2014	310	Daily	—
Anjum et al. [32]	Tianshan Mountains	IMERG-V06, IMERG-V05, TRMM3B42V7	June 2014–December 2017	37	Monthly, daily	Whole spatial area, climate zone
Chen et al. [44]	China	NCEP-2, CFSR, ERA-Interim, JRA-55, MERRA-2	1980–2014	817	Annual, monthly	Eastern and western regions
Fang et al. [45]	China	TRMM3B42, IMERG, IMERG-L, IMERG-E, GSMaP-N, GSMaP-M, TMPA-RT, PERSIANN-CCS, CMPA, PERSIANN-CCS, ERA5-Land, FY-4A, GSMaP, IMERG, CHIRPS, GPM-IMERG, PERSIANN-CCS	2000–2017	830	Annual	Whole spatial area
Chen et al. [13]	Global, China	IMERG, GSMaP-N, GSMaP-M, TMPA-RT, PERSIANN-CCS, CMPA, PERSIANN-CCS, ERA5-Land, FY-4A, GSMaP, IMERG, CHIRPS, GPM-IMERG, PERSIANN-CCS	February 2017–January 2019	17,000 (Global), 30,000 (China)	Daily, hourly	Global, China (whole spatial area, climate zone)
Gao et al. [33]	Southern China	IMERG, CHIRPS, GPM-IMERG, PERSIANN-CCS	June–August 2019	155	Daily, hourly	Administrative zone
Yu et al. [42]	China	SM2RASC, IMERG	2015–2017	553	Quarterly, monthly	Basin zone, topographic zone
Zhang et al. [43]	China	SM2RASC, IMERG	2012–2017	701	Monthly, daily	Climate zone

Table A1. Cont.

Source Documents	Research Region	Using Datasets	Research Timeline	Number of Stations	Time Dimension	Spatial Dimension
Tang et al. [49]	China	TRMM 3B42, CMORPH, PERSIANN-CDR, GSMaP, CHIRPS, SM2RAIN, ERA5, ERA-Interim, MERRA2, IMERG	2000–2018 (daily); Summer 2013–Summer 2015 (hourly)	2400 (daily); 30,000 (hourly)	Annual, quarterly, monthly, daily	Whole spatial area, Qinghai-Tibet Plateau, Xinjiang region, northeast region
Ren et al. [2]	Western China	FY-4A	June–August 2020	508	Hourly	Whole spatial area
Lu et al. [35]	Yunnan-Kweichow Plateau	CMPA, FY-4A	June–August 2019	323	Daily, hourly	Whole spatial area
Wei et al. [46]	China	IMERG-F, GSMaP-G, TMPA 3B42, CMORPH-CRT, PERSIANN-CDR, CHIRPS, IMERG-E, IMERG-L, GSMaP-RT, TMPA-RT, PERSIANN-RT, ERA5, ERA-Interim, MERRA2, GPCC, CPC, CRU	June 2000–December 2019	2400	Monthly	Climate zone
Jiang et al. [50]	China	IMERG-E, IMERG-L, IMERG-F	2001–2017	807	Monthly, daily	Whole spatial area, climate zone
Lilan Zhang et al. [12]	China	IMERG, GSMaP, MERRA, CFSR	2008–2017	2144	Quarterly, monthly, daily, hourly	Basin zone
Shaowei et al. [17]	Eastern China	CHIRPS, MSWEP, CMADS, PERSIANN-CDR, ITPCAS, AIMERG, CHIRPS, CMFD, ERA5-Land, IMERG, PERSIANN-CCS-CDR	2011–2015	2400	Quarterly, monthly, daily	Basin zone
Lele Zhang et al. [18]	Tibetan Plateau	IMERG, GSMaP, ERA5, ERA5-Land	2003–2015	143	Annual, monthly, daily	Whole spatial area
Xu et al. [39]	China	IMERG, GSMaP, ERA5, ERA5-Land	2016–2019	2200	Annual, monthly, daily, hourly	Climate zone
Yin et al. [41]	Northeast Asia	FY-2G, FY-4A, GK-2A	2020	304	Quarterly, hourly	Administrative zone
Lei et al. [47]	China	ERA5	1979–2020	666	Annual, monthly, daily	Geomorphologic regionalization
Liu [34]	Inner Tibetan Plateau	CHIRPS, CMORPH, GSMaP, IMERG, MSWEP, PERSIANN, TMPA, IMERG-E, IMERG-L, IMERG-F, GSMaP-G, GSMaP-N, GSMaP-GN	2014–2019	47	Annual, quarterly, monthly, daily	Whole spatial area
Weng et al. [48]	Xijiang River Basin	IMERG, GSMaP, ERA5, ERA5-Land	2009–2018	107	Annual, monthly, daily	—

## References

1. Hou, A.Y.; Kakar, R.K.; Neeck, S.; Azarbarzin, A.A.; Kummerow, C.D.; Kojima, M.; Oki, R.; Nakamura, K.; Iguchi, T. The Global Precipitation Measurement Mission. *Bull. Am. Meteorol. Soc.* **2014**, *95*, 701–722. [\[CrossRef\]](#)
2. Ren, J.; Xu, G.; Zhang, W.; Leng, L.; Xiao, Y.; Wan, R.; Wang, J. Evaluation and Improvement of FY-4A AGRI Quantitative Precipitation Estimation for Summer Precipitation over Complex Topography of Western China. *Remote Sens.* **2021**, *13*, 4366. [\[CrossRef\]](#)
3. Kidd, C.; Becker, A.; Huffman, G.J.; Muller, C.L.; Joe, P.; Skofronick-Jackson, G.; Kirschbaum, D.B. So, How Much of the Earth's Surface Is Covered by Rain Gauges? *Bull. Am. Meteorol. Soc.* **2017**, *98*, 69–78. [\[CrossRef\]](#) [\[PubMed\]](#)
4. Bathelemy, R.; Brigode, P.; Boisson, D.; Tric, E. Rainfall in the Greater and Lesser Antilles: Performance of five gridded datasets on a daily timescale. *J. Hydrol. Reg. Stud.* **2022**, *43*, 101203. [\[CrossRef\]](#)
5. Alsumaiti, T.S.; Hussein, K.; Ghebreyesus, D.T.; Sharif, H.O. Performance of the CMORPH and GPM IMERG Products over the United Arab Emirates. *Remote Sens.* **2020**, *12*, 1426. [\[CrossRef\]](#)
6. Arshad, M.; Ma, X.; Yin, J.; Ullah, W.; Ali, G.; Ullah, S.; Liu, M.; Shahzaman, M.; Ullah, I. Evaluation of GPM-IMERG and TRMM-3B42 precipitation products over Pakistan. *Atmos. Res.* **2021**, *249*, 105341. [\[CrossRef\]](#)
7. Huffman, G.J.; Bolvin, D.T.; Nelkin, E.J.; Wolff, D.B.; Adler, R.F.; Gu, G.; Hong, Y.; Bowman, K.P.; Stocker, E.F. The TRMM Multisatellite Precipitation Analysis (TMPA): Quasi-Global, Multiyear, Combined-Sensor Precipitation Estimates at Fine Scales. *J. Hydrometeorol.* **2007**, *8*, 38–55. [\[CrossRef\]](#)
8. Ning, S.; Zhou, H.-W.; Zhang, Z.-Y.; Bai, S.-B.; Liu, L. Precipitation scale effect of the TRMM satellite in Tianshan, China. *J. Mt. Sci.* **2023**, *20*, 1349–1368. [\[CrossRef\]](#)
9. Ma, Z.; Xu, J.; Zhu, S.; Yang, J.; Tang, G.; Yang, Y.; Shi, Z.; Hong, Y. AIMERG: A new Asian precipitation dataset (0.1°/half-hourly, 2000–2015) by calibrating the GPM-era IMERG at a daily scale using APHRODITE. *Earth Syst. Sci. Data* **2020**, *12*, 1525–1544. [\[CrossRef\]](#)
10. Yatagai, A.; Kamiguchi, K.; Arakawa, O.; Hamada, A.; Yasutomi, N.; Kitoh, A. APHRODITE: Constructing a Long-Term Daily Gridded Precipitation Dataset for Asia Based on a Dense Network of Rain Gauges. *Bull. Am. Meteorol. Soc.* **2012**, *93*, 1401–1415. [\[CrossRef\]](#)
11. Huffman, G.J.; Bolvin, D.T.; Braithwaite, D.; Hsu, K.-L.; Joyce, R.J.; Kidd, C.; Nelkin, E.J.; Sorooshian, S.; Stocker, E.F.; Tan, J.; et al. Integrated Multi-satellite Retrievals for the Global Precipitation Measurement (GPM) Mission (IMERG). In *Satellite Precipitation Measurement*; Levizzani, V., Kidd, C., Kirschbaum, D.B., Kummerow, C.D., Nakamura, K., Turk, F.J., Eds.; Springer International Publishing: Cham, Switzerland, 2020; Volume 67, pp. 343–353.
12. Zhang, L.; Chen, X.; Lai, R.; Zhu, Z. Performance of satellite-based and reanalysis precipitation products under multi-temporal scales and extreme weather in mainland China. *J. Hydrol.* **2022**, *605*, 127389. [\[CrossRef\]](#)
13. Chen, H.; Yong, B.; Shen, Y.; Liu, J.; Hong, Y.; Zhang, J. Comparison analysis of six purely satellite-derived global precipitation estimates. *J. Hydrol.* **2020**, *581*, 124376. [\[CrossRef\]](#)
14. Mega, T.; Ushio, T.; Kubota, T.; Kachi, M.; Aonashi, K.; Shige, S. Gauge adjusted global satellite mapping of precipitation (GSMaP\_Gauge). In Proceedings of the 2014 XXXIth URSI General Assembly and Scientific Symposium (URSI GASS), Beijing, China, 16–23 August 2014; pp. 1928–1935.
15. Hersbach, H.; Bell, B.; Berrisford, P.; Hirahara, S.; Horányi, A.; Muñoz-Sabater, J.; Nicolas, J.; Peubey, C.; Radu, R.; Schepers, D.; et al. The ERA5 global reanalysis. *Q. J. R. Meteorol. Soc.* **2020**, *146*, 1999–2049. [\[CrossRef\]](#)
16. Ma, Z.; Xu, J.; Ma, Y.; Zhu, S.; He, K.; Zhang, S.; Ma, W.; Xu, X. AERA5-Asia: A Long-Term Asian Precipitation Dataset (0.1°, 1-hourly, 1951–2015, Asia) Anchoring the ERA5-Land under the Total Volume Control by APHRODITE. *Bull. Am. Meteorol. Soc.* **2022**, *103*, E1146–E1171. [\[CrossRef\]](#)
17. Shaowei, N.; Jie, W.; Juliang, J.; Xiaoyan, X.; Yuliang, Z.; Fan, S.; Linlin, Z. Comprehensive evaluation of satellite-derived precipitation products considering spatial distribution difference of daily precipitation over eastern China. *J. Hydrol. Reg. Stud.* **2022**, *44*, 101242. [\[CrossRef\]](#)
18. Zhang, L.; Gao, L.; Chen, J.; Zhao, L.; Zhao, J.; Qiao, Y.; Shi, J. Comprehensive evaluation of mainstream gridded precipitation datasets in the cold season across the Tibetan Plateau. *J. Hydrol. Reg. Stud.* **2022**, *43*, 101186. [\[CrossRef\]](#)
19. Wang, C.; Tang, G.; Han, Z.; Guo, X.; Hong, Y. Global intercomparison and regional evaluation of GPM IMERG Version-03, Version-04 and its latest Version-05 precipitation products: Similarity, difference and improvements. *J. Hydrol.* **2018**, *564*, 342–356. [\[CrossRef\]](#)
20. Dehaghani, A.M.; Gohari, A.; Zareian, M.J.; Torabi Haghghi, A. A comprehensive evaluation of the satellite precipitation products across Iran. *J. Hydrol. Reg. Stud.* **2023**, *46*, 101360. [\[CrossRef\]](#)
21. Eini, M.R.; Olyaei, M.A.; Kamyab, T.; Teymoori, J.; Brocca, L.; Piniewski, M. Evaluating three non-gauge-corrected satellite precipitation estimates by a regional gauge interpolated dataset over Iran. *J. Hydrol. Reg. Stud.* **2021**, *38*, 100942. [\[CrossRef\]](#)
22. Ullah, W.; Wang, G.; Ali, G.; Tawia Hagan, D.; Bhatti, A.; Lou, D. Comparing Multiple Precipitation Products against in-Situ Observations over Different Climate Regions of Pakistan. *Remote Sens.* **2019**, *11*, 628. [\[CrossRef\]](#)
23. Purnadurga, G.; Kumar, T.V.L.; Rao, K.K.; Barbosa, H.; Mall, R.K. Evaluation of evapotranspiration estimates from observed and reanalysis data sets over Indian region. *Int. J. Climatol.* **2019**, *39*, 5791–5800. [\[CrossRef\]](#)
24. Wehbe, Y.; Ghebreyesus, D.; Temimi, M.; Milewski, A.; Al Mandous, A. Assessment of the consistency among global precipitation products over the United Arab Emirates. *J. Hydrol. Reg. Stud.* **2017**, *12*, 122–135. [\[CrossRef\]](#)

25. Ombadi, M.; Nguyen, P.; Sorooshian, S.; Hsu, K.I. Developing Intensity-Duration-Frequency (IDF) Curves From Satellite-Based Precipitation: Methodology and Evaluation. *Water Resour. Res.* **2018**, *54*, 7752–7766. [[CrossRef](#)]
26. Tarek, M.; Brissette, F.P.; Arsenault, R. Evaluation of the ERA5 reanalysis as a potential reference dataset for hydrological modelling over North America. *Hydrol. Earth Syst. Sci.* **2020**, *24*, 2527–2544. [[CrossRef](#)]
27. Islam, M.A.; Yu, B.; Cartwright, N. Assessment and comparison of five satellite precipitation products in Australia. *J. Hydrol.* **2020**, *590*, 125474. [[CrossRef](#)]
28. Montes, C.; Acharya, N.; Stiller-Reeve, M.A.; Kelley, C.; Hassan, S.M.Q. Interannual variability of monsoon onset and withdrawal in Bangladesh. *Atmos. Sci. Lett.* **2021**, *22*, e1069. [[CrossRef](#)]
29. Kourtis, I.M.; Bellos, V.; Zotou, I.; Vangelis, H.; Tsihrintzis, V.A. Point-to-pixel comparison of a satellite and a gauge-based Intensity-Duration-Frequency (IDF) curve: The case of Karditsa, Greece. In Proceedings of the 7th IAHR Europe Congress, Athens, Greece, 7–9 September 2022; pp. 267–268.
30. Chiaravalloti, F.; Brocca, L.; Procopio, A.; Massari, C.; Gabriele, S. Assessment of GPM and SM2RAIN-ASCAT rainfall products over complex terrain in southern Italy. *Atmos. Res.* **2018**, *206*, 64–74. [[CrossRef](#)]
31. Gentilucci, M.; Barbieri, M.; Pambianchi, G. Reliability of the IMERG product through reference rain gauges in Central Italy. *Atmos. Res.* **2022**, *278*, 106340. [[CrossRef](#)]
32. Anjum, M.N.; Ahmad, I.; Ding, Y.; Shangguan, D.; Zaman, M.; Ijaz, M.W.; Sarwar, K.; Han, H.; Yang, M. Assessment of IMERG-V06 Precipitation Product over Different Hydro-Climatic Regimes in the Tianshan Mountains, North-Western China. *Remote Sens.* **2019**, *11*, 2314. [[CrossRef](#)]
33. Gao, Z.; Huang, B.; Ma, Z.; Chen, X.; Qiu, J.; Liu, D. Comprehensive Comparisons of State-of-the-Art Gridded Precipitation Estimates for Hydrological Applications over Southern China. *Remote Sens.* **2020**, *12*, 3997. [[CrossRef](#)]
34. Liu, Z. Accuracy of satellite precipitation products in data-scarce Inner Tibetan Plateau comprehensively evaluated using a novel ground observation network. *J. Hydrol. Reg. Stud.* **2023**, *47*, 101405. [[CrossRef](#)]
35. Lu, H.; Huang, Z.; Ding, L.; Lu, T.; Yuan, Y. Calibrating FY4A QPE using CMPA over Yunnan–Kweichow Plateau in summer 2019. *Eur. J. Remote Sens.* **2021**, *54*, 476–486. [[CrossRef](#)]
36. Qin, Y.; Chen, Z.; Shen, Y.; Zhang, S.; Shi, R. Evaluation of Satellite Rainfall Estimates over the Chinese Mainland. *Remote Sens.* **2014**, *6*, 11649–11672. [[CrossRef](#)]
37. Shen, Y.; Zhao, P.; Pan, Y.; Yu, J. A high spatiotemporal gauge-satellite merged precipitation analysis over China. *J. Geophys. Res. Atmos.* **2014**, *119*, 3063–3075. [[CrossRef](#)]
38. Tang, G.; Zeng, Z.; Long, D.; Guo, X.; Yong, B.; Zhang, W.; Hong, Y. Statistical and Hydrological Comparisons between TRMM and GPM Level-3 Products over a Midlatitude Basin: Is Day-1 IMERG a Good Successor for TMPA 3B42V7? *J. Hydrometeorol.* **2016**, *17*, 121–137. [[CrossRef](#)]
39. Xu, J.; Ma, Z.; Yan, S.; Peng, J. Do ERA5 and ERA5-land precipitation estimates outperform satellite-based precipitation products? A comprehensive comparison between state-of-the-art model-based and satellite-based precipitation products over mainland China. *J. Hydrol.* **2022**, *605*, 127353. [[CrossRef](#)]
40. Yang, Y.; Luo, Y. Evaluating the performance of remote sensing precipitation products CMORPH, PERSIANN, and TMPA, in the arid region of northwest China. *Theor. Appl. Climatol.* **2014**, *118*, 429–445. [[CrossRef](#)]
41. Yin, G.; Baik, J.; Park, J. Comprehensive analysis of GEO-KOMPSAT-2A and FengYun satellite-based precipitation estimates across Northeast Asia. *GIScience Remote Sens.* **2022**, *59*, 782–800. [[CrossRef](#)]
42. Yu, C.; Hu, D.; Liu, M.; Wang, S.; Di, Y. Spatio-temporal accuracy evaluation of three high-resolution satellite precipitation products in China area. *Atmos. Res.* **2020**, *241*, 104952. [[CrossRef](#)]
43. Zhang, L.; Li, X.; Cao, Y.; Nan, Z.; Wang, W.; Ge, Y.; Wang, P.; Yu, W. Evaluation and integration of the top-down and bottom-up satellite precipitation products over mainland China. *J. Hydrol.* **2020**, *581*, 124456. [[CrossRef](#)]
44. Chen, S.; Gan, T.Y.; Tan, X.; Shao, D.; Zhu, J. Assessment of CFSR, ERA-Interim, JRA-55, MERRA-2, NCEP-2 reanalysis data for drought analysis over China. *Clim. Dyn.* **2019**, *53*, 737–757. [[CrossRef](#)]
45. Fang, J.; Yang, W.; Luan, Y.; Du, J.; Lin, A.; Zhao, L. Evaluation of the TRMM 3B42 and GPM IMERG products for extreme precipitation analysis over China. *Atmos. Res.* **2019**, *223*, 24–38. [[CrossRef](#)]
46. Wei, L.; Jiang, S.; Ren, L.; Wang, M.; Zhang, L.; Liu, Y.; Yuan, F.; Yang, X. Evaluation of seventeen satellite-, reanalysis-, and gauge-based precipitation products for drought monitoring across mainland China. *Atmos. Res.* **2021**, *263*, 105813. [[CrossRef](#)]
47. Lei, X.; Xu, W.; Chen, S.; Yu, T.; Hu, Z.; Zhang, M.; Jiang, L.; Bao, R.; Guan, X.; Ma, M.; et al. How Well Does the ERA5 Reanalysis Capture the Extreme Climate Events Over China? Part I: Extreme Precipitation. *Front. Environ. Sci.* **2022**, *10*, 921658. [[CrossRef](#)]
48. Weng, P.; Tian, Y.; Jiang, Y.; Chen, D.; Kang, J. Assessment of GPM IMERG and GSMaP daily precipitation products and their utility in droughts and floods monitoring across Xijiang River Basin. *Atmos. Res.* **2023**, *286*, 10667. [[CrossRef](#)]
49. Tang, G.; Clark, M.P.; Papalexiou, S.M.; Ma, Z.; Hong, Y. Have satellite precipitation products improved over last two decades? A comprehensive comparison of GPM IMERG with nine satellite and reanalysis datasets. *Remote Sens. Environ.* **2020**, *240*, 111697. [[CrossRef](#)]
50. Jiang, S.; Wei, L.; Ren, L.; Xu, C.-Y.; Zhong, F.; Wang, M.; Zhang, L.; Yuan, F.; Liu, Y. Utility of integrated IMERG precipitation and GLEAM potential evapotranspiration products for drought monitoring over mainland China. *Atmos. Res.* **2021**, *247*, 105141. [[CrossRef](#)]

51. Yong, B.; Chen, B.; Tian, Y.; Yu, Z.; Hong, Y. Error-Component Analysis of TRMM-Based Multi-Satellite Precipitation Estimates over Mainland China. *Remote Sens.* **2016**, *8*, 440. [[CrossRef](#)]
52. Zhang, Y.; Long, H.; Chen, S.; Ma, L.; Gan, M. The development of multifunctional agriculture in farming regions of China: Convergence or divergence? *Land Use Policy* **2023**, *127*, 106576. [[CrossRef](#)]
53. Xiao, S.; Zou, L.; Xia, J.; Yang, Z.; Yao, T. Bias correction framework for satellite precipitation products using a rain/no rain discriminative model. *Sci. Total Environ.* **2022**, *818*, 151679. [[CrossRef](#)]
54. Kummerow, C.D.; Randel, D.L.; Kulie, M.; Wang, N.-Y.; Ferraro, R.; Joseph Munchak, S.; Petkovic, V. The Evolution of the Goddard Profiling Algorithm to a Fully Parametric Scheme. *J. Atmos. Ocean. Technol.* **2015**, *32*, 2265–2280. [[CrossRef](#)]
55. Pipunic, R.C.; Ryu, D.; Costelloe, J.F.; Su, C.-H. An evaluation and regional error modeling methodology for near-real-time satellite rainfall data over Australia. *J. Geophys. Res. Atmos.* **2015**, *120*, 10767–10783. [[CrossRef](#)]

**Disclaimer/Publisher’s Note:** The statements, opinions and data contained in all publications are solely those of the individual author(s) and contributor(s) and not of MDPI and/or the editor(s). MDPI and/or the editor(s) disclaim responsibility for any injury to people or property resulting from any ideas, methods, instructions or products referred to in the content.